

Higgs photon associated production in a Two Higgs Doublet Type-II Seesaw Model at future electron-positron colliders.

B. Ait Ouazghour,^{1*} M. Chabab^{1†} K. Goure^{1‡}

¹ LPHEA, Faculty of Science Semlalia, Cadi Ayyad University, P.O.B. 2390 Marrakech, Morocco.

Abstract

We study the one-loop prediction for the single production of a SM-like Higgs boson in association with a photon in electron-positron collisions in the context of the two Higgs doublet type-II seesaw model ($2HDMcT$). We explore to what extent the new scalars in the $2HDMcT$ spectrum affect its production cross-section, the ratio $R_{\gamma h_1}$ as well as the signal strengths $R_{\gamma Z}$ and $R_{\gamma\gamma}$ when h_1 is identified with the observed SM Higgs boson within the $2HDMcT$ delimited parameter space. More specifically, we focus on $e^+e^- \rightarrow h_1\gamma$ process at one-loop, and analyzed how it evolves under a full set of theoretical constraints and the available experimental data, including $B \rightarrow X_s\gamma$ limit at 95% C.L. Our analysis shows that these observables are strongly dependent on the parameters of the model, especially the mixing angle α_1 , the potential parameters λ_7, λ_9 , the trilinear Higgs couplings, with a noticeable sensitivity to α_1 . We found that $\sigma(e^+e^- \rightarrow h_1\gamma)$ can significantly be enhanced up to 8.1×10^{-2} fb, thus exceeding the Standard Model prediction. Additionally, as a byproduct, we also observed that $R_{\gamma h_1}$ is entirely correlated with both the $h_1 \rightarrow \gamma\gamma$ and $h_1 \rightarrow \gamma Z$ signal strengths.

1 Introduction

The discovery of the Higgs boson, the last missing piece in the completion of the Standard Model (SM), by the ATLAS [1] and CMS [2] collaborations provided an experimental evidence for the Brout-Englert-Higgs mechanism. Since then, major ongoing studies have focused on exploring in detail the properties of the Higgs boson with the aim to enhance our understanding of the fundamental laws of nature. Although most of the SM 's predictions have been tested successfully to a high level of accuracy [3–5], it still suffers from drawbacks since it failed to explain several established physical phenomena. As examples, the origin of dark matter [6,7], the hierarchy problem [8], and the neutrino mass generation [9,10] do not fit in the SM .

To address these issues, a plethora of new physics models have been proposed in literature. Among these beyond the Standard Model (BSM), scenarios relying on an extended Higgs sectors with new scalar fields, as the popular two Higgs Doublet Model ($2HDM$) [11–16], the Higgs Triplet Models (HTM) [14,16] and recently $2HDM$ augmented by a complex triplet scalar, dubbed the two Higgs Doublet Type-II Seesaw Model ($2HDMcT$) [17,18]. Since the spectra of these models generally predict additional Higgs bosons with novel features, searching for these new scalars has been actively conducted as a key focus and one of the major motivations for the current and future experiments, especially at LHC [19–25]. Besides, as no direct evidence for new physics has been seen yet, precision measurements of the Higgs boson properties and couplings [26–30] to other new scalars can offer a promising opportunity for a potential discovery of new physics. Indeed, more accurate understanding of the Higgs boson and the measurements of its couplings with high levels of precision is the main goal of future e^+e^- colliders [31] such as the International Linear Collider (ILC) [32,33], Compact Linear Collider (CLIC) [31,34], Circular Electron-Positron Collider (CEPC) [35–37], and Future Circular Collider (FCC) [38,39]. Compared to hadron colliders, these colliders, featuring a cleaner e^+e^- background, can yield substantial improvements over LHC measurements [40].

*brahim.aitouazghour@edu.uca.ac.ma

†mchabab@uca.ac.ma (corresponding author)

‡k.goure.ced@uca.ac.ma

The associated production of the SM-like Higgs boson with a photon, $e^+e^- \rightarrow h_1\gamma$ is well suited to study the Higgs-gauge bosons couplings such as the $h_1\gamma\gamma$ and $h_1\gamma Z$ couplings. Since the production rate can be sizably amplified in the presence of new physics contributions as compared to the SM, this process may serve as a potential discovery channel. This process was investigated in the SM [41–43] and recently in some *BSM* scenarios as the inert Higgs doublet model [44], *HTM* [45], the minimal supersymmetric standard model (MSSM) [46, 47] and the effective field theory [48].

In this work, we investigate the single production of the neutral Higgs boson in association with a photon in electron positron collisions within the Two Higgs Doublet Type II Seesaw Model (*2HDMcT*). To do that, we implement a full set of theoretical constraints originated from perturbative unitarity, electroweak vacuum stability, as well as the experimental Higgs exclusion limits from LEP, LHC and Tevatron. Since the mass generation from seesaw mechanism is similar to the Brout-Englert-Higgs mechanism, *2HDMcT* model is appealing, displaying many phenomenological features especially different from those emerging in *2HDM* scalar sector. Apart its broader spectrum than *2HDM*'s one, the doubly charged Higgs H^{++} , as a smoking gun of *2HDMcT*, H^{++} is currently intensively searched for at ATLAS and CMS, by means of promising decay channels, such as $H^{++}H^{--}$ and $H_i^+H_i^-$ ($i = 1, 2$), decaying to the same sign di-lepton [17]. Furthermore, *2HDMcT* is arguably one of the simplest frameworks that can account for both the dark matter issue [49] as well as the neutrino mass problem [50–52]. Along side the doubly charged Higgs the phenomenological features of this model include the possibility of enhanced Higgs couplings, modified Higgs decay channels, and the presence of additional scalar particles that can be probed at the Large Hadron Collider (LHC) or other future colliders. For example one of the prospective signals that can be probed is $pp \rightarrow Z/\gamma \rightarrow H_2^+H_2^- \rightarrow H^{++}W^-H^{--}W^+ \rightarrow l^+l^+l^-l^- + 4j$. This process does not show up neither in *2HDM* nor in *HTM* giving that the mass splitting $\Delta m = m_{H^{++}} - m_{H^+}$ is constrained by the oblique parameters to be less than 40 GeV in *HTM* [53]. New contribution to the oblique parameters from the new states in *2HDMcT* makes this avoidable. Additionally, beyond Higgs phenomenology, it has been demonstrated that interactions between doublet and triplet fields may induce a strong first order electroweak phase transition, which provide conditions for the generation of the baryon asymmetry through electroweak baryogenesis [54].

This paper is organized as follows: In Sect. 2, we briefly review *2HDMcT* model and mention some theoretical and experimental constraints imposed on the model parameter space. In Sect. 3 we study the two processes $e^+e^- \rightarrow h_1\gamma$ and $e^-\gamma \rightarrow h_1e^-$ in *2HDMcT* and discuss the correlation of the signal strengths for the one loop induced processes $h_1 \rightarrow \gamma\gamma$ and $h_1 \rightarrow Z\gamma$ in *2HDMcT*. Sect. 4 is devoted to our conclusion.

2 Two Higgs Doublet Type-II Seesaw Model: Brief overview

2HDMcT has recently gained interest as a well-motivated extension of the *2HDM*. Besides the two Higgs doublets with hypercharge $Y = +1$, *2HDM* is augmented with one colorless triplet field Δ transforming under the $SU(2)_L$ gauge group as a complex scalar with $Y_\Delta = 2$.

$$\Phi_1 = \begin{pmatrix} \phi_1^+ \\ \phi_1^0 \end{pmatrix}, \quad \Phi_2 = \begin{pmatrix} \phi_2^+ \\ \phi_2^0 \end{pmatrix} \quad \text{and} \quad \Delta = \begin{pmatrix} \delta^+/\sqrt{2} & \delta^{++} \\ (v_t + \delta^0 + i\eta_0)/\sqrt{2} & -\delta^+/\sqrt{2} \end{pmatrix} \quad (1)$$

with $\phi_1^0 = (v_1 + \psi_1 + i\eta_1)/\sqrt{2}$, $\phi_2^0 = (v_2 + \psi_2 + i\eta_2)/\sqrt{2}$. v_1, v_2 and v_t denote the vacuum expectation values of the Higgs doublets and triplet fields respectively, acquired when the electroweak symmetry is spontaneously broken, with $\sqrt{v_1^2 + v_2^2 + 2v_t^2} = 246$ GeV. Consequently, eleven physical Higgs states occur in the model spectrum: three CP-even neutral Higgs bosons (h_1, h_2, h_3), four simply

charged Higgs bosons (H_1^\pm, H_2^\pm), two CP odd Higgs bosons (A_1, A_2), and finally two doubly charged Higgs bosons $H^{\pm\pm}$. For details see [17].

The most general $SU(2)_L \times U(1)_Y$ invariant scalar potential in this model reads : [13, 17]:

$$\begin{aligned}
V(\Phi_1, \Phi_2, \Delta) &= m_{11}^2 \Phi_1^\dagger \Phi_1 + m_{22}^2 \Phi_2^\dagger \Phi_2 - [m_{12}^2 \Phi_1^\dagger \Phi_2 + \text{h.c.}] + \frac{\lambda_1}{2} (\Phi_1^\dagger \Phi_1)^2 + \frac{\lambda_2}{2} (\Phi_2^\dagger \Phi_2)^2 \\
&+ \lambda_4 (\Phi_1^\dagger \Phi_2)(\Phi_2^\dagger \Phi_1) + \left\{ \frac{\lambda_5}{2} (\Phi_1^\dagger \Phi_2)^2 + [\beta_1 (\Phi_1^\dagger \Phi_1) + \beta_2 (\Phi_2^\dagger \Phi_2)] \Phi_1^\dagger \Phi_2 + \text{h.c.} \right\} \\
&+ \lambda_3 (\Phi_1^\dagger \Phi_1)(\Phi_2^\dagger \Phi_2) + \lambda_6 \Phi_1^\dagger \Phi_1 \text{Tr} \Delta^\dagger \Delta + \lambda_7 \Phi_2^\dagger \Phi_2 \text{Tr} \Delta^\dagger \Delta \\
&+ \left\{ \mu_1 \Phi_1^T i \sigma^2 \Delta^\dagger \Phi_1 + \mu_2 \Phi_2^T i \sigma^2 \Delta^\dagger \Phi_2 + \mu_3 \Phi_1^T i \sigma^2 \Delta^\dagger \Phi_2 + \text{h.c.} \right\} + \lambda_8 \Phi_1^\dagger \Delta \Delta^\dagger \Phi_1 \\
&+ \lambda_9 \Phi_2^\dagger \Delta \Delta^\dagger \Phi_2 + m_\Delta^2 \text{Tr}(\Delta^\dagger \Delta) + \bar{\lambda}_8 (\text{Tr} \Delta^\dagger \Delta)^2 + \bar{\lambda}_9 \text{Tr}(\Delta^\dagger \Delta)^2 \tag{2}
\end{aligned}$$

In this work we assume that $m_{11}^2, m_{22}^2, m_\Delta^2, m_{12}^2, \lambda_{1,2,3,4,5,6,7,8,9}, \bar{\lambda}_{8,9}, \mu_{1,2,3}, \beta_{1,2}$ are real parameters. To avoid tree-level Higgs mediated $FCNC_s$ at tree level, we consider Z_2 symmetry where $\beta_1 = \beta_2 = 0$. Also the Z_2 symmetry is softly broken by the bi-linear terms proportional to m_{12}^2, μ_1, μ_2 and μ_3 parameters. Thanks to the combination $v^2 = v_1^2 + v_2^2 + 2v_t^2 = (2\sqrt{2}G_F)^{-1}$ and the three minimization conditions, the scalar potential Eq. (2) has seventeen independent parameters, one possible choice is :

$$\alpha_1, \alpha_2, \alpha_3, m_{h_1}, m_{h_2}, m_{h_3}, m_{H^{\pm\pm}}, \lambda_1, \lambda_3, \lambda_4, \lambda_6, \lambda_8, \bar{\lambda}_8, \bar{\lambda}_9, \mu_1, v_t \text{ and } \tan \beta$$

where $\alpha_{i=1,2,3}$ are the CP-even mixing angles and $\tan \beta = v_2/v_1$.

In our subsequent analysis h_1 is identified to the SM-like Higgs boson with $m_{H^{SM}} = 125$ GeV [1, 2]. So the scalar potential is described by sixteen free parameters. The Yukawa lagrangian $\mathcal{L}_{\text{Yukawa}}$ contains all the Yukawa sector of the Two Higgs Doublet Model plus one extra Yukawa term emerging from the triplet field and generating a small Majorana mass terms for the neutrinos when the symmetry is spontaneously broken.

$$-\mathcal{L}_{\text{Yukawa}} \supset -Y_\nu L^T C \otimes i \sigma^2 \Delta L + \text{h.c.} \tag{3}$$

For the type II 2HDMcT, up quarks interact with Φ_2 , while leptons and down quarks with Φ_1 as :

$$-\mathcal{L}_{\text{Yukawa}}^{II} = -y_u \bar{Q}_L \tilde{\Phi}_2 u_R - y_d \bar{Q}_L \Phi_1 d_R - y_\ell \bar{L}_L \Phi_1 \ell_R + \text{h.c.}, \tag{4}$$

Here Q_L and L_L represent the left-handed quark and lepton doublets, $u_R, d_R,$ and ℓ_R are the right-handed up-type quarks, down-type quarks, and lepton singlets. Φ_1 and Φ_2 are the two Higgs doublets, with $\tilde{\Phi}_2 = i \sigma_2 \Phi_2^*$. $y_u, y_d,$ and y_ℓ are the Yukawa couplings for the up, down-type quarks and leptons, respectively. The Yukawa couplings of the CP-even Higgs bosons h_i to fermions are presented in Table 1. The matrix elements \mathcal{E}_{ij} are given in Appendix B.1.

ϕ	ξ_ϕ^u	ξ_ϕ^d	ξ_ϕ^ℓ
h_1	$\frac{\mathcal{E}_{12}}{s_\beta}$	$-\frac{\mathcal{E}_{11}}{c_\beta}$	$-\frac{\mathcal{E}_{11}}{c_\beta}$
h_2	$\frac{\mathcal{E}_{22}}{s_\beta}$	$-\frac{\mathcal{E}_{21}}{c_\beta}$	$-\frac{\mathcal{E}_{21}}{c_\beta}$
h_3	$\frac{\mathcal{E}_{32}}{s_\beta}$	$-\frac{\mathcal{E}_{31}}{c_\beta}$	$-\frac{\mathcal{E}_{31}}{c_\beta}$

Table 1: Yukawa couplings of the $h_1, h_2,$ and h_3 bosons to the quarks and leptons in 2HDMcT

2.1 Theoretical and Experimental Constraints

The phenomenological analysis in $2HDMcT$ is performed via implementation of a full set of theoretical constraints [17, 18] as well as the Higgs exclusion limits from various experimental measurements at colliders, namely :

- **Unitarity** : The scattering processes must obey perturbative unitarity.
- **Perturbativity**: The quartic couplings of the scalar potential are constrained by the following conditions : $|\lambda_i| < 8\pi$ for each $i = 1, \dots, 5$.
- **Vacuum stability** : Boundedness from below BFB arising from the positivity in any direction of the fields Φ_i, Δ .
- **Electroweak precision observables**: The oblique parameters S, T and U [55, 56] have been calculated in $2HDMcT$ [18]. The analysis of the precision electroweak data in light of the new PDG mass of the W boson yields [57]:

$$\widehat{S}_0 = -0.01 \pm 0.07, \quad \widehat{T}_0 = 0.04 \pm 0.06, \quad \rho_{ST} = 0.92,$$

We use the following χ_{ST}^2 test :

$$\frac{(S - \widehat{S}_0)^2}{\sigma_S^2} + \frac{(T - \widehat{T}_0)^2}{\sigma_T^2} - 2\rho_{ST} \frac{(S - \widehat{S}_0)(T - \widehat{T}_0)}{\sigma_S \sigma_T} \leq R^2 (1 - \rho_{ST}^2), \quad (5)$$

with $R^2 = 2.3$ and 5.99 corresponding to 68.3% and 95% confidence levels (C.L.) respectively. Our numerical analysis is performed with χ_{ST}^2 at 95% C.L.

- To further delimit the allowed parameter space, the `HiggsTools` package [58] is employed. This ensures that the allowed parameter regions align with the observed properties of the 125 GeV Higgs boson (`HiggsSignals` [58–61]) and with the limits from searches for additional Higgs bosons at the LHC and at LEP (`HiggsBounds` [58, 62–65]).
- **Flavour constraints**: Flavour constraints are also implemented in our analysis. We used B -physics results, derived in [18] as well as the experimental data at 2σ [66] displayed in Table 2.

Observable	Experimental result	95% C.L.
$\text{BR}(\bar{B} \rightarrow X_s \gamma)$ [18]	$(3.49 \pm 0.19) \times 10^{-4}$ [66]	$[3.11 \times 10^{-4}, 3.87 \times 10^{-4}]$

Table 2: Experimental result of flavor observable: $\bar{B} \rightarrow X_s \gamma$ at 95% C.L.

3 $e^+e^- \rightarrow \gamma h_1$ and $e^- \gamma \rightarrow e^- h_1$ in $2HDMcT$

3.1 Process topology

The $e^+e^- \rightarrow \gamma h_1$ process has been studied in many of beyond the Standard Model frameworks. In the $2HDMcT$, at tree level, the associated production processes $e^+e^- \rightarrow \gamma h_1$ and $e^- \gamma \rightarrow e^- h_1$ are intermediated by the t-channel and s-channel electron exchange diagrams respectively. However, the former diagrams are suppressed by the electron mass. At one-loop these diagrams are mediated by the self-energy, box, and triangle diagrams and hence are sensitive to all virtual particles inside the loops including the charged Higgs states, H_1^\pm, H_2^\pm and $H^{\pm\pm}$, predicted by our model.

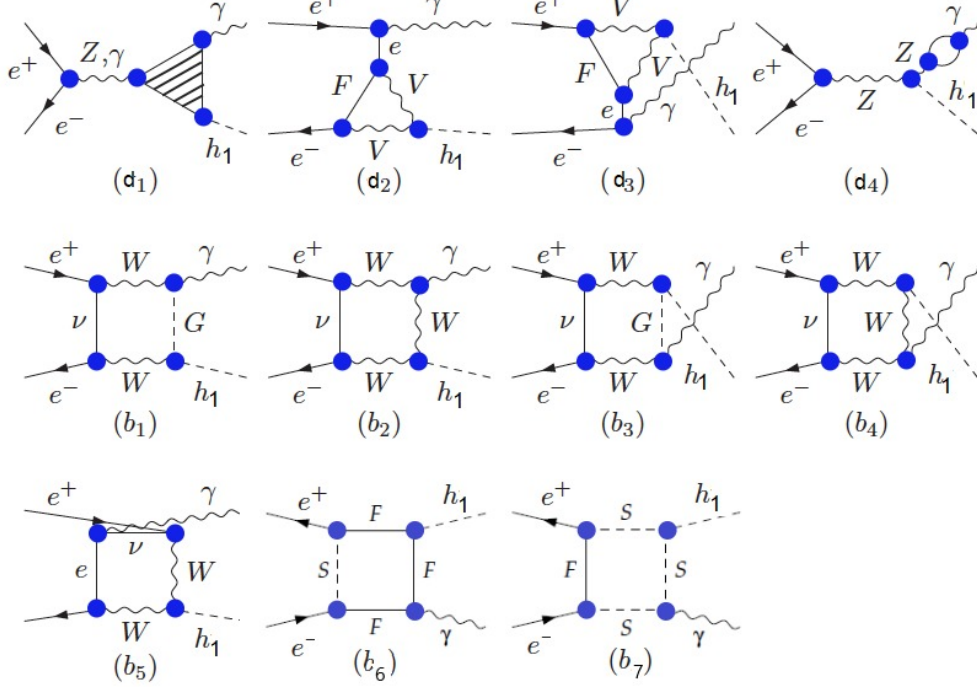


Figure 1: Feynman diagrams involving the charged contributions to $e^-e^+ \rightarrow \gamma h_1$ process in 2HDMcT. In d_1 , d_4 , b_6 and b_7 diagrams, the loops receive contributions from SM particles as well as the charged Higgs bosons H_1^\pm , H_2^\pm and $H^{\pm\pm}$. Generic diagrams d_2, d_3 , depict $h_1 V V$, $V = \gamma, Z$.

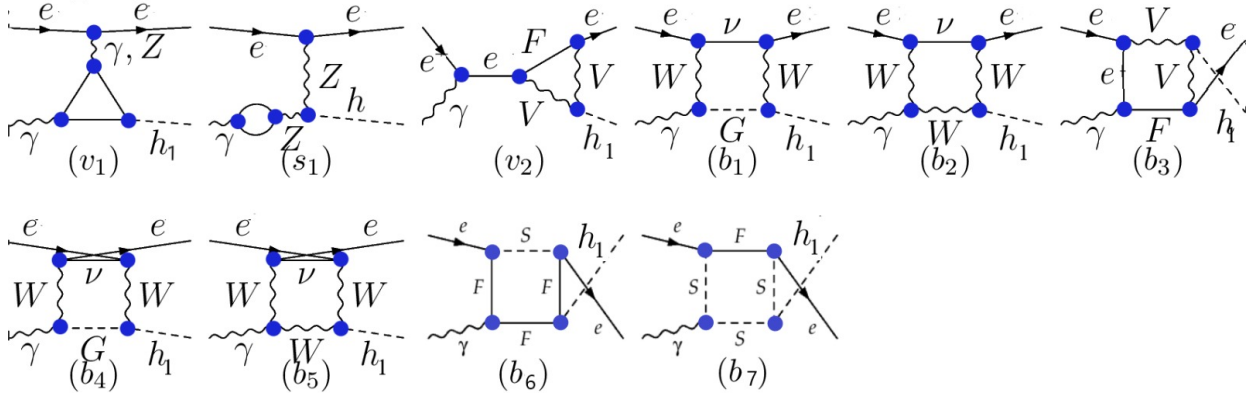


Figure 2: Feynman diagrams involving the charged contributions to $e^-\gamma \rightarrow e^-h_1$ process in the 2HDMcT. In diagrams v_1 , we depict all possible charged particles. Diagrams s_1 , b_6 and b_7 depict the contributions from H_1^\pm , H_2^\pm and $H^{\pm\pm}$ bosons.

Figs. 1, 2 and 3 illustrate the generic Feynman diagrams that effectively contribute to the $e^+e^- \rightarrow \gamma h_1$, $e^-\gamma \rightarrow e^-h_1$ and $h_1 \rightarrow \gamma V$ processes, with $V = \gamma, Z$. Here F stands for any fermionic particle, while S denotes the charged states H_1^\pm , H_2^\pm and $H^{\pm\pm}$.

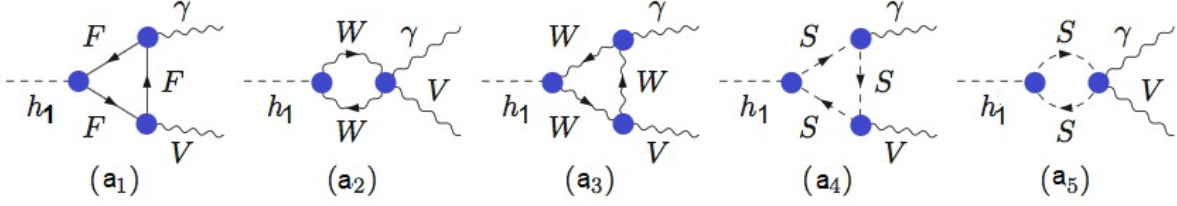


Figure 3: Feynman diagrams for the decay process $h_1 \rightarrow \gamma V$ ($V = \gamma, Z$) in the $2HDMcT$. a_4, a_5 illustrate the contributions of the charged Higgses H_1^\pm, H_2^\pm and $H^{\pm\pm}$.

Summing over the polarization of the photon, the differential cross section of the Higgs associated production with a photon is calculated using the the generic formula :

$$\frac{d\sigma}{d\cos\theta}(e^+e^- \rightarrow h_1\gamma) = \frac{s - m_{h_1}^2}{32\pi s^2} \sum_{pol} |\mathcal{M}|^2, \quad (6)$$

where \sqrt{s} is the center-of-mass energy of e^+e^- collisions and θ is the scattering angle between the photon and the electron in the centre-of-mass frame.

The total amplitudes for the process can be expressed as a sum over all contributions from triangle, box, and self-energy diagrams.

$$\mathcal{M} = \mathcal{M}_\Delta + \mathcal{M}_\square + \mathcal{M}_\circ \quad (7)$$

- \mathcal{M}_Δ : Contains s-channel γ and Z exchange vertex diagrams that involve virtual W and heavy fermion loops. The significant contributions from these fermion loops arise mainly from top and bottom quark loops, as the Yukawa couplings to lighter fermions are very small. Also t-channel vertex diagrams involving W /neutrino and Z /electron exchanges (corrections to the $h_1 e^+ e^-$ vertex).
- \mathcal{M}_\square : The box diagrams get contribution from W /neutrino and Z /electron diagrams.
- \mathcal{M}_\circ : Include SM loops contributions from charged fermions and W bosons.
- Additionally $\mathcal{M}_{\Delta, \square, \circ}$ also receive contributions from the new charged scalars, namely, H_1^\pm, H_2^\pm and $H^{\pm\pm}$ as illustrated in Fig. 1.

The integrated cross section over all θ angles is given by

$$\sigma(e^+e^- \rightarrow h_1\gamma) = \int_{-1}^{+1} d\cos\theta \frac{d\sigma}{d\cos\theta}. \quad (8)$$

Our calculation is performed using dimensional regularization along with *FeynArts* and *FormCalc* packages [67, 68]. while the numerical evaluation of the scalar integrals is done with *LoopTools* [69, 70]. Note that the gauge invariance of our final results is assured once contributions from all box and triangle diagrams are summed. In the subsequent analysis, we introduce the ratio,

$$R_{\gamma h_1} \equiv \frac{\sigma(e^+e^- \rightarrow \gamma h_1)}{\sigma(e^+e^- \rightarrow \gamma H^{\text{SM}})} \quad (9)$$

which is the total cross-section in the $2HDMcT$ normalized to the SM one. Also we define the diphoton and γZ gauge bosons signal strengths, $R_{\gamma\gamma}$ and $R_{Z\gamma}$,

$$R_{\gamma\gamma(Z\gamma)} \equiv \frac{\sigma(gg \rightarrow h_1) \times Br(h_1 \rightarrow \gamma\gamma(Z\gamma))}{\sigma(gg \rightarrow H^{\text{SM}}) \times Br(H^{\text{SM}} \rightarrow \gamma\gamma(Z\gamma))} \quad (10)$$

The decay width for $h_1 \rightarrow \gamma\gamma$ and $h_1 \rightarrow \gamma Z$ in 2HDMcT are given by,

$$\Gamma(h_1 \rightarrow \gamma\gamma) = \frac{G_F \alpha^2 M_{h_1}^3}{128 \sqrt{2} \pi^3} \left| \sum_f N_c Q_f^2 k_f A_{1/2}^{h_1}(\tau_f) + \lambda_{h_1 WW} A_1^{h_1}(\tau_W) + \tilde{\lambda}_{h_1 H_1^\pm H_1^\mp} A_0^{h_1}(\tau_{H_1^\pm}) + \tilde{\lambda}_{h_1 H_2^\pm H_2^\mp} A_0^{h_1}(\tau_{H_2^\pm}) + 4 \tilde{\lambda}_{h_1 H^{\pm\pm} H^{\mp\mp}} A_0^{h_1}(\tau_{H^{\pm\pm}}) \right|^2 \quad (11)$$

$$\Gamma(h_1 \rightarrow Z\gamma) = \frac{G_\mu^2 M_W^2 \alpha M_{h_1}^3}{64 \pi^4} \left(1 - \frac{M_Z^2}{M_{h_1}^2} \right)^3 \left| \sum_f \frac{Q_f \hat{v}_f N_c}{c_W} k_f \mathcal{F}_{1/2}^{h_1}(\tau_f, \lambda_f) + \lambda_{WW} \mathcal{F}_1^{h_1}(\tau_W, \lambda_W) + \lambda_{ZH_1^\pm H_1^\mp} \tilde{\lambda}_{h_1 H_1^\pm H_1^\mp} \mathcal{F}_0^{h_1}(\tau_{H_1^\pm}, \lambda_{H_1^\pm}) + \lambda_{ZH_2^\pm H_2^\mp} \tilde{\lambda}_{h_1 H_2^\pm H_2^\mp} \mathcal{F}_0^{h_1}(\tau_{H_2^\pm}, \lambda_{H_2^\pm}) + \lambda_{ZH^{\pm\pm} H^{\mp\mp}} \tilde{\lambda}_{h_1 H^{\pm\pm} H^{\mp\mp}} \mathcal{F}_0^{h_1}(\tau_{H^{\pm\pm}}, \lambda_{H^{\pm\pm}}) \right|^2 \quad (12)$$

where $\tilde{\lambda}_{h_1 H_i^\pm H_i^\mp} = \lambda_{h_1 H_i^\pm H_i^\mp} \times \frac{M_W^2}{M_{H_i^\pm}^2}$, $i=1,2$ and $\tilde{\lambda}_{h_1 H^{\pm\pm} H^{\mp\mp}} = \lambda_{h_1 H^{\pm\pm} H^{\mp\mp}} \times \frac{M_W^2}{M_{H^{\pm\pm}}^2}$. The functions $A_{1/2}^{h_1}(\tau_i)$, $A_1^{h_1}(\tau_i)$, $A_0^{h_1}(\tau_i)$, $\mathcal{F}_0^{h_1}(\tau_{H^i}, \lambda_{H^i})$, $\mathcal{F}_1^{h_1}(\tau_W, \lambda_W)$ and $\mathcal{F}_{1/2}^{h_1}(\tau_f, \lambda_f)$ are defined in Appendix A. The reduced couplings $\lambda_{h_1 ff}$ and $\lambda_{h_1 WW}$ of the Higgs bosons to fermions and W bosons are displayed in Tables 1 and 3 respectively. $\lambda_{ZH_1^\pm H_1^\mp}$, $\lambda_{ZH_2^\pm H_2^\mp}$ and $\lambda_{ZH^{\pm\pm} H^{\mp\mp}}$ are given in Eqs. 29 Compared

	$C_W^{h_i}$	$C_Z^{h_i}$
h_1	$\frac{v_1}{v} \mathcal{E}_{11} + \frac{v_2}{v} \mathcal{E}_{21} + 2 \frac{v_t}{v} \mathcal{E}_{31}$	$\frac{v_1}{v} \mathcal{E}_{11} + \frac{v_2}{v} \mathcal{E}_{21} + 4 \frac{v_t}{v} \mathcal{E}_{31}$
h_2	$\frac{v_1}{v} \mathcal{E}_{12} + \frac{v_2}{v} \mathcal{E}_{22} + 2 \frac{v_t}{v} \mathcal{E}_{32}$	$\frac{v_1}{v} \mathcal{E}_{12} + \frac{v_2}{v} \mathcal{E}_{22} + 4 \frac{v_t}{v} \mathcal{E}_{32}$
h_3	$\frac{v_1}{v} \mathcal{E}_{13} + \frac{v_2}{v} \mathcal{E}_{23} + 2 \frac{v_t}{v} \mathcal{E}_{33}$	$\frac{v_1}{v} \mathcal{E}_{13} + \frac{v_2}{v} \mathcal{E}_{23} + 4 \frac{v_t}{v} \mathcal{E}_{33}$

Table 3: The normalized couplings of the neutral \mathcal{CP}_{even} h_i Higgs to the massive gauge bosons $V = W, Z$ in 2HDMcT. The matrix elements \mathcal{E}_{ij} are given in Eq. 34

with the Standard Model, the amplitudes for the loop processes $e^- \gamma \rightarrow e^- h_1$, $e^+ e^- \rightarrow \gamma h_1$ and $h_1 \rightarrow \gamma V$ ($V = \gamma, Z$) receive additional contributions from the charged Higgs bosons predicted in the model spectrum H_1^\pm , H_2^\pm and $H^{\pm\pm}$. These amplitudes are essentially proportional to the couplings with h_1 Higgs boson,

$$\begin{aligned} \tilde{\lambda}_{h_1 H_1^\pm H_1^\mp} &= \frac{s_w}{2em_w} (2\mathcal{C}_{21}^2 (\lambda_6 \mathcal{E}_{13} v_\Delta + \lambda_1 v_1 \mathcal{E}_{11} + \lambda_3 v_2 \mathcal{E}_{12}) \\ &\quad + 2\mathcal{C}_{22}^2 (\lambda_7 \mathcal{E}_{13} v_\Delta + \lambda_2 v_2 \mathcal{E}_{12} + \lambda_3 v_1 \mathcal{E}_{11}) \\ &\quad + \mathcal{C}_{23}^2 (2\mathcal{E}_{13} (2\bar{\lambda}_8 + \bar{\lambda}_9) v_\Delta + (2\lambda_6 + \lambda_8) v_1 \mathcal{E}_{11} + (2\lambda_7 + \lambda_9) v_2 \mathcal{E}_{12}) \\ &\quad + \mathcal{C}_{22} \mathcal{C}_{23} (\sqrt{2} \lambda_9 \mathcal{E}_{12} v_\Delta + \sqrt{2} \lambda_9 v_2 \mathcal{E}_{13} - 4\mu_2 \mathcal{E}_{12} - 2\mu_3 \mathcal{E}_{11}) \\ &\quad + \mathcal{C}_{21} (\mathcal{C}_{23} (\sqrt{2} \lambda_8 \mathcal{E}_{11} v_\Delta + \sqrt{2} \lambda_8 v_1 \mathcal{E}_{13} - 4\mu_1 \mathcal{E}_{11} - 2\mu_3 \mathcal{E}_{12}) \\ &\quad + 2\mathcal{C}_{22} (\lambda_4 + \lambda_5) (v_2 \mathcal{E}_{11} + v_1 \mathcal{E}_{12})) \end{aligned} \quad (14)$$

$$\tilde{\lambda}_{h_1 H_2^\pm H_2^\mp} = \frac{s_w}{2em_w} (2\mathcal{C}_{31}^2 (\lambda_6 \mathcal{E}_{13} v_\Delta + \lambda_1 v_1 \mathcal{E}_{11} + \lambda_3 v_2 \mathcal{E}_{12}))$$

$$\begin{aligned}
& +2\mathcal{C}_{32}^2 (\lambda_7 \mathcal{E}_{13} v_\Delta + \lambda_2 v_2 \mathcal{E}_{12} + \lambda_3 v_1 \mathcal{E}_{11}) \\
& +\mathcal{C}_{33}^2 (2\mathcal{E}_{13} (2\bar{\lambda}_8 + \bar{\lambda}_9) v_\Delta + (2\lambda_6 + \lambda_8) v_1 \mathcal{E}_{11} + (2\lambda_7 + \lambda_9) v_2 \mathcal{E}_{12}) \\
& +\mathcal{C}_{32} \mathcal{C}_{33} \left(\sqrt{2} \lambda_9 \mathcal{E}_{12} v_\Delta + \sqrt{2} \lambda_9 v_2 \mathcal{E}_{13} - 4\mu_2 \mathcal{E}_{12} - 2\mu_3 \mathcal{E}_{11} \right) \\
& +\mathcal{C}_{31} \left(\mathcal{C}_{33} \left(\sqrt{2} \lambda_8 \mathcal{E}_{11} v_\Delta + \sqrt{2} \lambda_8 v_1 \mathcal{E}_{13} - 4\mu_1 \mathcal{E}_{11} - 2\mu_3 \mathcal{E}_{12} \right) \right. \\
& \left. +2\mathcal{C}_{32} (\lambda_4 + \lambda_5) (v_2 \mathcal{E}_{11} + v_1 \mathcal{E}_{12}) \right)
\end{aligned} \tag{15}$$

$$\bar{\lambda}_{h_1 H^{\pm\pm} H^{\pm\pm}} = \frac{s_w}{em_w} (2\bar{\lambda}_8 \mathcal{E}_{13} v_\Delta + \lambda_6 v_1 \mathcal{E}_{11} + \lambda_7 v_2 \mathcal{E}_{12}) \tag{16}$$

At this stage it is worth noticing that:

- These couplings are mostly fixed by α_1 , λ_3 , λ_4 , λ_7 and λ_9 parameters when $\tan \beta$ takes relatively large values, since $v_t \ll v_1 < v_2$.
- Depending on their signs, the charged Higgs contributions can either enhance or suppress the $e^+e^- \rightarrow \gamma h_1$ and $h_1 \rightarrow \gamma V$ rates ($V = \gamma, Z$).

3.2 Results and analysis

Given that h_1 is identified as the SM-like Higgs boson, observed at the LHC with $m_{h_1} = 125$ GeV, we perform scans within the allowed parameter space by implementation of the theoretical and experimental constraints mentioned above.

The following set of input parameters is used in the subsequent numerical analysis :

$$\mathcal{P}_I = \{ \alpha_1, \alpha_2, \alpha_3, m_{h_1}, m_{h_2}, \lambda_1, \lambda_3, \lambda_4, \lambda_6, \lambda_7, \lambda_8, \lambda_9, \bar{\lambda}_8, \bar{\lambda}_9, \mu_1, v_t, \tan \beta \} \tag{17}$$

$$\begin{aligned}
& m_{h_1} = 125 \text{ GeV}, \quad m_{h_1} \leq m_{h_2} \leq m_{h_3} \leq 1 \text{ TeV}, \quad 80 \text{ GeV} \leq m_{H_1^\pm}, m_{H_2^\pm}, m_{H^{\pm\pm}} \leq 1 \text{ TeV}, \\
& -2\pi \leq \lambda_1 \leq 2\pi, \quad -2\pi \leq \lambda_{3,4} \leq 2\pi, \quad -2\pi \leq \lambda_{6,7} \leq 2\pi, \quad -2\pi \leq \lambda_{8,9} \leq 2\pi, \quad -2\pi \leq \bar{\lambda}_{8,9} \leq 2\pi \\
& -\pi/2 \leq \alpha_1 \leq \pi/2, \quad \alpha_2 \approx 0, \quad \alpha_3 \approx 0, \quad \mu_1 = v_t = 1 \text{ GeV}, \quad \tan \beta = 8
\end{aligned} \tag{18}$$

Since $v_t \ll v_1 < v_2$, we can see from equations (14), (15), and (16), that the virtual charged states H_1^\pm , H_2^\pm impact on $h_1 \gamma \gamma$ and $h_1 \gamma Z$ couplings induce a dependence on λ_3 , λ_4 , λ_7 and λ_9 , with a noticeable sensitivity to α_1 . The doubly charged Higgs $H^{\pm\pm}$ instead leads to λ_7 dependence and to α_1 strong sensitivity. Comparatively, the influence of the other model parameters is either mild or negligible.

In Fig. 4, we show the allowed ranges for (λ_7, λ_9) as well as the size of the trilinear couplings $\bar{\lambda}_{h_1 H_1^\pm H_1^\pm}$, $\bar{\lambda}_{h_1 H_2^\pm H_2^\pm}$ and $\bar{\lambda}_{h_1 H^{\pm\pm} H^{\pm\pm}}$. All generated points passed upon the full set of constraints at 2σ . The upper panel displays the charged Higgs masses $m_{H_1^\pm}$ (left), $m_{H_2^\pm}$ (middle) and $m_{H^{\pm\pm}}$ (right) in the (λ_7, λ_9) plane. We can clearly see that λ_7 and λ_9 drastically reduce to $0 < \lambda_7 < 2\pi$ and $-5.25 < \lambda_9 < 1.01$ due to the combination of the BFB conditions with the Higgs exclusion limits implemented in **HiggsTools**. One can also notice that λ_7 and λ_9 have opposite effects on the trilinear couplings, as illustrated by the middle and lower panels in Fig. 4: λ_7 increases $\bar{\lambda}_{h_1 H^{\pm\pm} H^{\pm\pm}}$, $\bar{\lambda}_{h_1 H_1^\pm H_1^\pm}$, $\bar{\lambda}_{h_1 H_2^\pm H_2^\pm}$, while λ_9 weakens these trilinear couplings. Similarly compatibility with all the constraints oblige the parameters $\mu_{2,3}$ to undergo drastic reductions being confined within the mitigated intervals, $0 \text{ GeV} < \mu_2 < 8 \text{ GeV}$ and $70 \text{ GeV} < \mu_3 < 108 \text{ GeV}$ respectively.

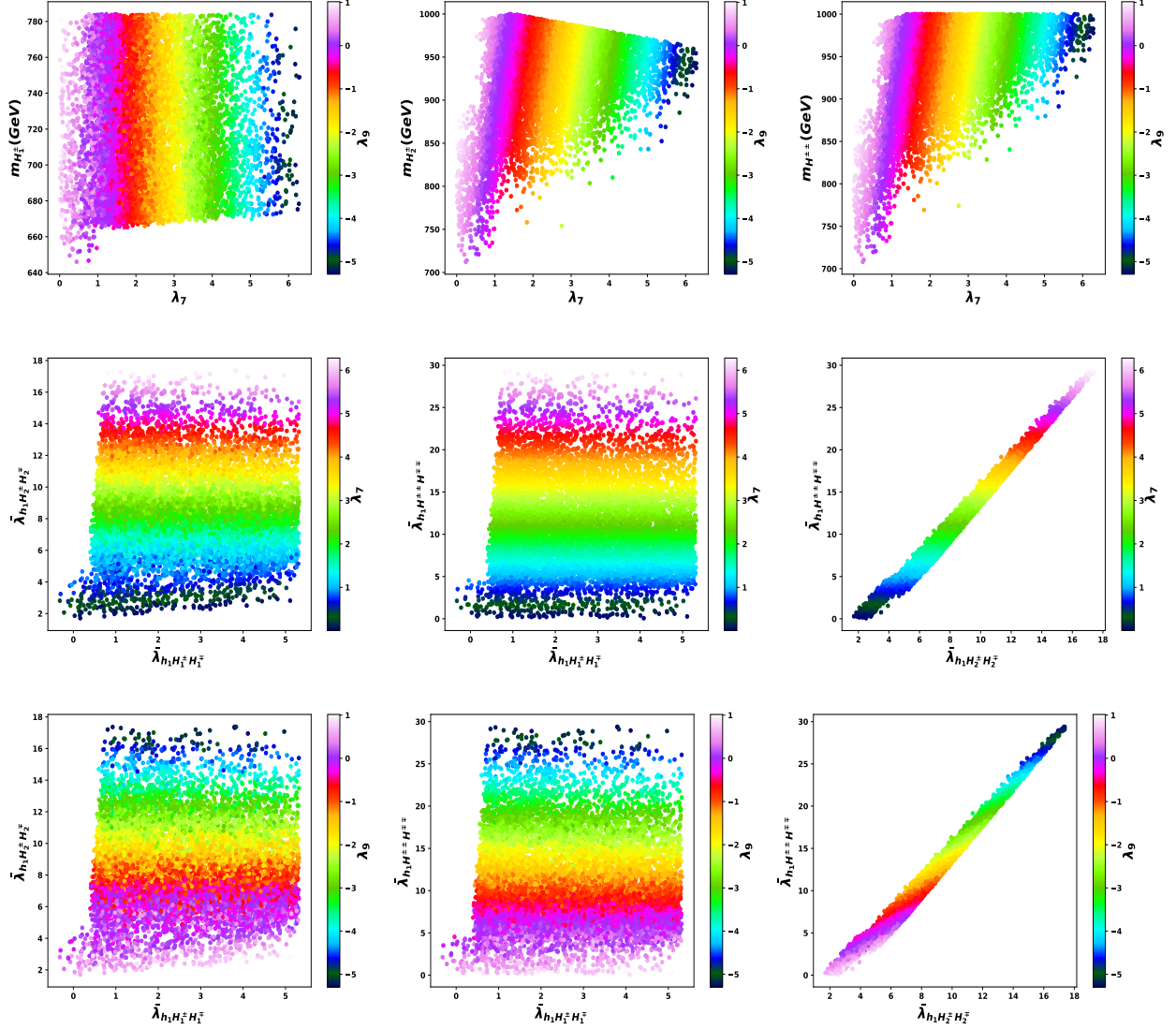


Figure 4: Upper panels: The charged Higgs masses as a function of λ_7 and λ_9 with $m_{H_1^\pm}$ (left), $m_{H_2^\pm}$ (middle) and $m_{H^{\pm\pm}}$ (right). Middle panels: correlation between $\bar{\lambda}_{h_1 H_1^\pm H_1^\mp}$ and $\bar{\lambda}_{h_1 H_2^\pm H_2^\mp}$ (left), $\bar{\lambda}_{h_1 H_1^\pm H_1^\mp}$ and $\bar{\lambda}_{h_1 H^{\pm\pm} H^{\mp\mp}}$ (middle), $\bar{\lambda}_{h_1 H_2^\pm H_2^\mp}$ and $\bar{\lambda}_{h_1 H^{\pm\pm} H^{\mp\mp}}$ (right) as a function of λ_7 . Lower panels: correlation between $\bar{\lambda}_{h_1 H_1^\pm H_1^\mp}$ and $\bar{\lambda}_{h_1 H_2^\pm H_2^\mp}$ (left), $\bar{\lambda}_{h_1 H_1^\pm H_1^\mp}$ and $\bar{\lambda}_{h_1 H^{\pm\pm} H^{\mp\mp}}$ (middle), $\bar{\lambda}_{h_1 H_2^\pm H_2^\mp}$ and $\bar{\lambda}_{h_1 H^{\pm\pm} H^{\mp\mp}}$ (right) as a function of λ_9 . Here we assume that $\alpha_1 = 1.42$ and $m_{h_2} = 673.30$ GeV. The other inputs are the same as in (18). The analysis is performed with χ^2_{ST} test where only points that are within 95% C.L. are considered.

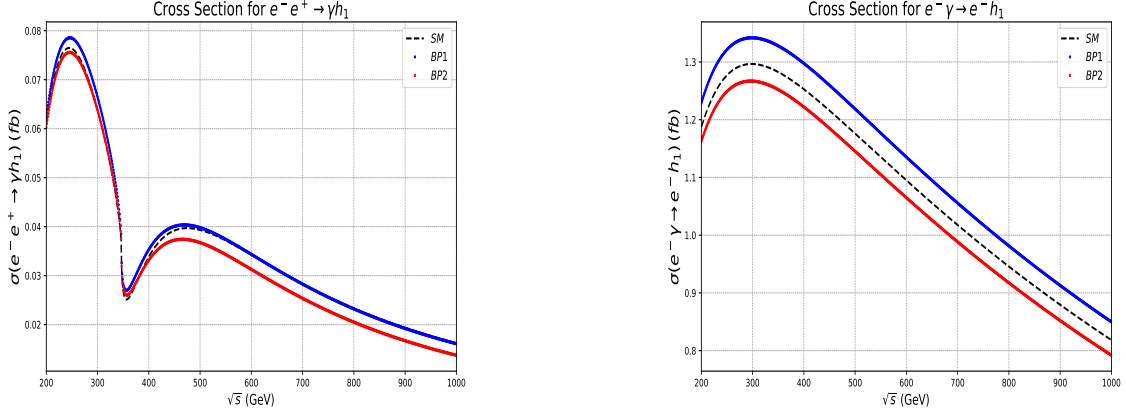


Figure 5: Total unpolarized cross-sections in fb for $e^+e^- \rightarrow \gamma h_1$ (left) and $e^-\gamma \rightarrow e^- h_1$ (right) as a function of center-of-mass energy, in two benchmark scenarios. Here we assume that $\alpha_1 = 1.42$ and $m_{h_2} = 673.30$ GeV. The other inputs are displayed in Table 4.

Fig. 5 displays the unpolarized cross sections of $e^-e^+ \rightarrow h_1\gamma$ and $e^-\gamma \rightarrow e^-h_1$ in 2HDMcT as a function of \sqrt{s} in the range 200 to 1000 GeV. These cross sections at the linear collider are analyzed in two benchmark scenarios illustrated in Table 4. We see that the $\sigma(e^-e^+ \rightarrow h_1\gamma)$ is significantly enhanced near $\sqrt{s} = 250$ GeV, however as \sqrt{s} increases the cross section decreases until reaching a local minimum around $t\bar{t}$ threshold $\sqrt{s} \approx 346$ GeV. This is a general trend of the cross section seen in SM, and in many extended Higgs sector models [44, 45]. In comparison to SM, the interference between the SM and the new 2HDMcT contributions can either be constructive or destructive, thus implying an increase or a decrease of the cross section. From Eq. 6 in our paper, one can readily see that the cross section for $\sigma(e^-e^+ \rightarrow h_1\gamma)$ scales like $1/s$ for large \sqrt{s} , hence explaining the decrease in this cross section at high \sqrt{s} .

As for $\sigma(e^-\gamma \rightarrow e^-h_1)$ decay, it shows a slower decrease at high values of energy, due essentially to the t-channel contribution. At this point, we must stress that the interference between 2HDMcT and SM contributions is sensitive to the couplings $\bar{\lambda}_{h_1 H^{\pm\pm} H^{\mp\mp}}$, $\bar{\lambda}_{h_1 H_1^\pm H_1^\pm}$, and $\bar{\lambda}_{h_1 H_2^\pm H_2^\pm}$. From Eqs (14, 15, 16). we see that these trilinear Higgs couplings are expressed in terms of several potential parameters. However our analysis finds that $e^-e^+ \rightarrow h_1\gamma$ and $e^-\gamma \rightarrow e^-h_1$ cross sections are mainly dependent on λ_3 , λ_7 and λ_9 , with a noticeable sensitivity α_1 .

Table 4: Benchmark scenarios used in Fig. 5 where the generated points pass upon the full set of constraints.

Bench.	λ_1	λ_3	λ_4	λ_6	λ_7	λ_8	λ_9	$\bar{\lambda}_8$	$\bar{\lambda}_9$
BP1	1.31	-0.12	1.70	0.64	0.01	0.28	0.38	2.33	0.54
BP2	1.31	0.80	3.06	6.04	2.15	-2.72	0.47	-1.10	3.13

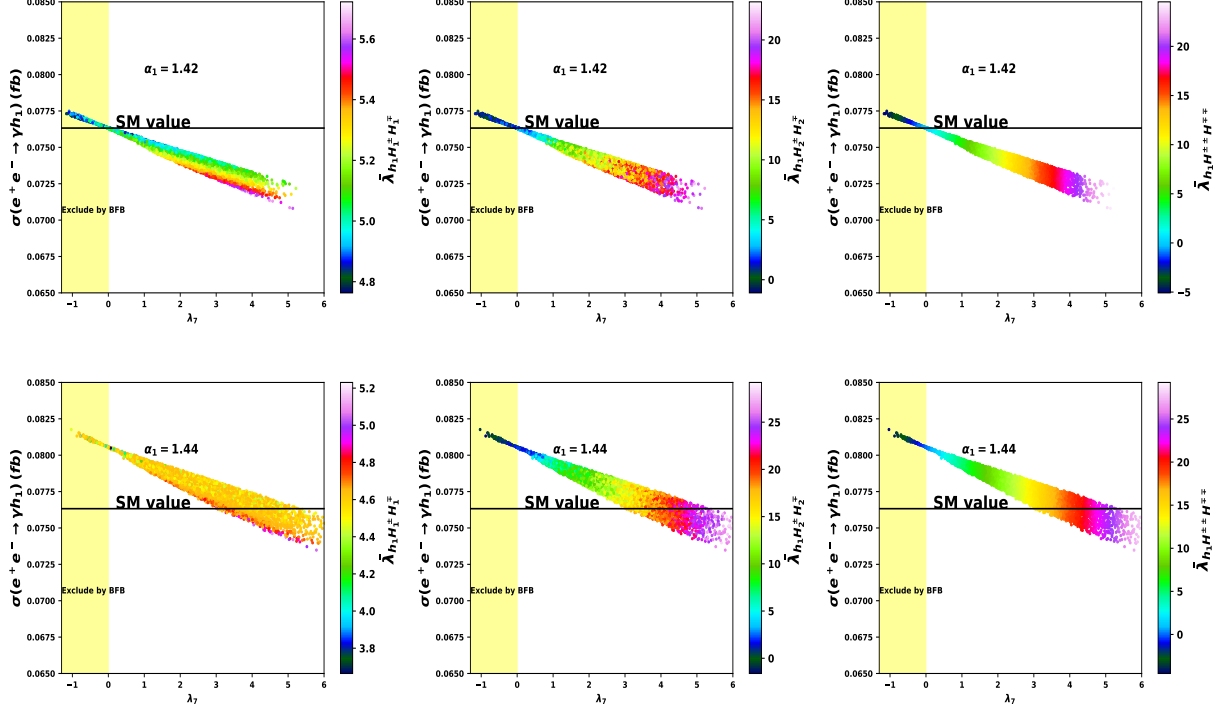


Figure 6: The cross-section $\sigma(e^+e^- \rightarrow \gamma h_1)$ is depicted as a function of the parameter λ_7 for two values of the parameter α_1 : $\alpha_1 = 1.42$ (upper panels), and $\alpha_1 = 1.44$ (lower panels). The plotted points pass upon all constraints. We used : $\lambda_1 = 1.31$, $\lambda_3 = 6.15$, $\lambda_4 = -3.85$ and $m_{h_2} = 673.30$ GeV. The other inputs are the same as in (18). The color coding illustrates the variation of the trilinear couplings $\bar{\lambda}_{h_1 H_1^\pm H_1^\mp}$ (left), $\bar{\lambda}_{h_1 H_2^\pm H_2^\mp}$ (middle) and $\bar{\lambda}_{h_1 H^{++} H^{--}}$ (right panel)

Next, we first aim to see whether the diphoton signal strength $R_{\gamma\gamma}(h_1)$ agrees with the experimental data within the model's parameter space, knowing that, unlike $h_1 \rightarrow \gamma Z$ process, the decay channel $h_1 \rightarrow \gamma\gamma$, has been measured with high precision [3, 4, 71–75]. Also, we want to analyze to what extent the cross-section $\sigma(e^+e^- \rightarrow \gamma h_1)$ behavior is affected either by the $2HDMcT$ charged Higgs bosons or by the potential parameters. Fig. 6 and Fig. 7 illustrate the variation of these observables as a function of the parameter λ_7 , and the trilinear couplings $\bar{\lambda}_{h_1 H_1^+ H_1^-}$, $\bar{\lambda}_{h_1 H_2^+ H_2^-}$ and $\bar{\lambda}_{h_1 H^{++} H^{--}}$. It is generally observed that an increase in λ_7 results in a detrimental effect on both $R_{\gamma\gamma}$ and $\sigma(e^+e^- \rightarrow \gamma h_1)$. Similar trend is seen if these observables are plotted versus λ_3 .

In Fig. 6 we plot the cross section of $e^+e^- \rightarrow \gamma h_1$ as a function of the parameter λ_7 , and the trilinear Higgs couplings for two nearly degenerate values of the parameter α_1 . From the upper panels, with $\alpha_1 = 1.42$, we clearly see that $\sigma(e^+e^- \rightarrow \gamma h_1)$ undergoes a notable increase and even exceeds the SM prediction if $\lambda_7 < 0$, a region excluded by the *BFB* constraints. In this scenario, because of *BFB* conditions, the contributions of the parameters $\lambda_{6,7,8,9,\bar{8},\bar{9}}$ are rather predominantly detrimental, inducing a decrease in $\sigma(e^+e^- \rightarrow \gamma h_1)$. More specifically this depreciation stems particularly from the relations, $\lambda_7 > 0$ and $\lambda_7 + \lambda_9 > 0$, with λ_7 and λ_9 exhibiting contrasting effects. However, if we consider a slightly larger value of the parameter $\alpha_1 = 1.44$, as illustrated by the lower panels, the cross section experience a significant enhancement and can well surpass that of the SM up to 8.1×10^{-2} fb, while still satisfying BFB conditions. This underscores the strong sensitivity to α_1 . In addition, as a byproduct, our analysis also show that the charged Higgs masses $m_{H_1^\pm}$, $m_{H_2^\pm}$ and $m_{H^{\pm\pm}}$ are compelled to lie within the very stringent intervals [785, 790] GeV, [807, 990] GeV and [810, 995] GeV respectively, confirming the predictions reported in [18].

Next we analyze the signal strengths $R_{\gamma\gamma}$, $R_{\gamma Z}$ and the ratio $R_{\gamma h_1}$ within the model parameter space. First, we plot in Fig.7 the signal strength of the Higgs to diphoton decay as a function of the parameter λ_7 , so we observe that $R_{\gamma\gamma}$ is clearly consistent with the measured signal strength [3, 4, 71–75] at 1σ .

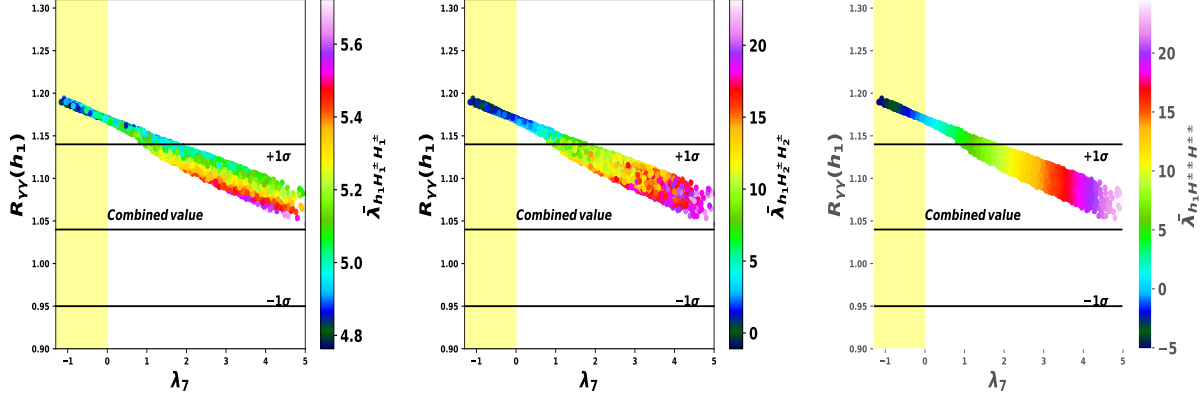


Figure 7: The signal strength $R_{\gamma\gamma}(h_1)$ as a function of λ_7 . The plotted points passed upon all constraints. The color coding shows the variation of the trilinear coupling $\bar{\lambda}_{h_1 H_1^\pm H_1^\mp}$ (left), $\bar{\lambda}_{h_1 H_2^\pm H_2^\mp}$ (middle) and $\bar{\lambda}_{h_1 H^{\pm\pm} H^{\mp\mp}}$ (right panel). The displayed horizontal lines denote the central and $\pm 1\sigma$ diphoton signal strength values reported by ATLAS at 13 TeV [4, 71]. We used the following inputs: $\alpha_1 = 1.42$, $\lambda_1 = 1.31$, $\lambda_3 = 6.15$, $\lambda_4 = -3.85$ and $m_{h_2} = 673.30$ GeV. The other inputs are the same as in (18), while the error for χ^2 fit is 95% C.L.

Then, we investigate how $R_{\gamma h_1}$ behaves with respect to $R_{\gamma\gamma}$ and $R_{\gamma Z}$ and whether these observables are correlated. One can readily see from Fig. 8 a clear correlation with these two signal strengths. Additionally, we also analyzed the incidence of the doubly charged Higgs on these loop induced processes, via its trilinear Higgs couplings $\bar{\lambda}_{h_1 H^{\pm\pm} H^{\mp\mp}}$. Interestingly the results indicate that the lighter it is, the more significant the enhancement in $\sigma(e^+e^- \rightarrow \gamma h_1)$, as in $R_{\gamma h_1}$ and $R_{\gamma Z}$.

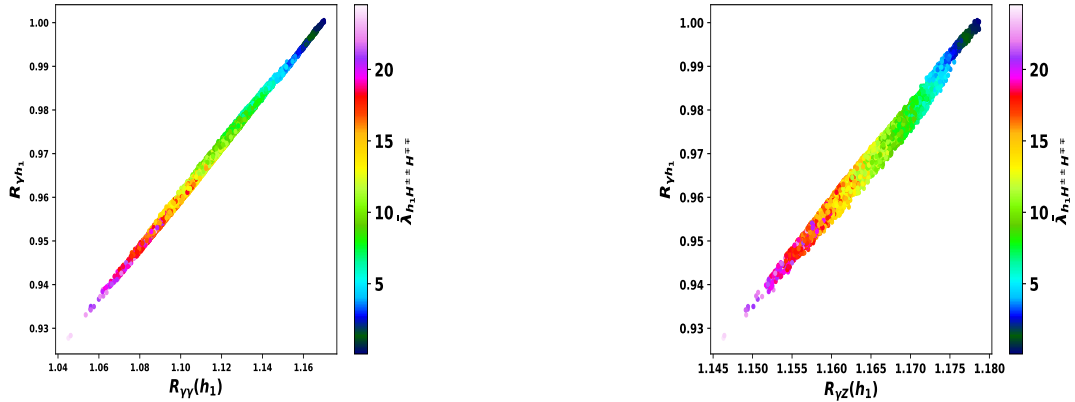


Figure 8: $R_{\gamma h_1}$ correlation with $R_{\gamma\gamma}(h_1)$ (left panels) and $R_{\gamma Z}(h_1)$ (right panels) in $2HDMcT$. Color coding shows the variation of $\bar{\lambda}_{h_1 H^{\pm\pm} H^{\mp\mp}}$. The other inputs are the same as in Fig. 7.

4 CONCLUSION

The future e^-e^+ colliders are anticipated to play a vital role in understanding the nature of the Higgs boson and its coupling to the SM particles with unprecedented precision. In the present paper, we have studied the one-loop processes $e^+e^- \rightarrow \gamma h_1$ and $e^- \gamma \rightarrow e^- h_1$ with a more focus on $e^+e^- \rightarrow \gamma h_1$ in the framework of $2HDMcT$ at the e^-e^+ colliders, where the h_1 Higgs boson is chosen to replicate the observed Higgs. Within the $2HDMcT$ parameter space delimited by a full set of constraints, we have shown that the $2HDMcT$ charged scalars can substantially alter the cross sections $\sigma(e^+e^- \rightarrow \gamma h_1)$ and $\sigma(e^- \gamma \rightarrow e^- h_1)$. Our analysis also observed that these observables are strongly dependent on the model parameters, especially α_1 , λ_7 , λ_9 , and the trilinear Higgs couplings, with a particularly strong sensitivity to α_1 . These parameters conspire to induce significant contributions to $\sigma(e^+e^- \rightarrow h_1 \gamma)$, up to 8.1×10^{-2} fb thus exceeding the SM prediction.

Furthermore, the charged scalars H_1^\pm , H_2^\pm and $H^{\pm\pm}$ also affected the ratio $R_{h_1\gamma}$ and the signal strength $R_{Z\gamma}$, while $R_{\gamma\gamma}$ being consistent with the measured signal strength at 1σ . At last, our analysis showed that these three observables are entirely correlated with each other.

Appendices

A Decay width functions

Here we present the definition of the functions appearing in the Higgs decay widths.

$$\begin{aligned} A_{1/2}^{h_1}(\tau) &= 2[\tau + (\tau - 1)f(\tau)] \tau^{-2} \\ A_1^{h_1}(\tau) &= -[2\tau^2 + 3\tau + 3(2\tau - 1)f(\tau)] \tau^{-2} \\ A_0^{h_1}(\tau) &= -[\tau - f(\tau)] \tau^{-2} \end{aligned} \quad (19)$$

The scaling variables are defined as $\tau_i = M_\Phi^2/4M_i^2$, where M_i represents the loop mass. The function $f(\tau)$ is defined as,

$$f(\tau) = \begin{cases} \arcsin^2 \sqrt{\tau} & \tau \leq 1 \\ -\frac{1}{4} \left[\log \frac{1 + \sqrt{1 - \tau^{-1}}}{1 - \sqrt{1 - \tau^{-1}}} - i\pi \right]^2 & \tau > 1 \end{cases} \quad (20)$$

$$\mathcal{F}_{1/2}^{h_1}(\tau, \lambda) = [I_1(\tau, \lambda) - I_2(\tau, \lambda)] \quad (21)$$

$$\mathcal{F}_1^{h_1}(\tau, \lambda) = c_W \left\{ 4 \left(3 - \frac{s_W^2}{c_W^2} \right) I_2(\tau, \lambda) + \left\{ \left(1 + \frac{2}{\tau} \right) \frac{s_W^2}{c_W^2} - \left(5 + \frac{2}{\tau} \right) \right\} I_1(\tau, \lambda) \right\} \quad (22)$$

with $\hat{v}_f = 2I_f^3 - 4Q_f s_W^2$. The functions I_1 et I_2 are given by,

$$I_1(\tau, \lambda) = \frac{\tau\lambda}{2(\tau - \lambda)} + \frac{\tau^2\lambda^2}{2(\tau - \lambda)^2} [f(\tau^{-1}) - f(\lambda^{-1})] + \frac{\tau^2\lambda}{(\tau - \lambda)^2} [g(\tau^{-1}) - g(\lambda^{-1})] \quad (23)$$

$$I_2(\tau, \lambda) = -\frac{\tau\lambda}{2(\tau - \lambda)} [f(\tau^{-1}) - f(\lambda^{-1})] \quad (24)$$

. the function $f(\tau)$ is defined above in Eq. (20) whereas the $g(\tau)$ function can be expressed as,

$$g(\tau) = \begin{cases} \sqrt{\tau^{-1} - 1} \arcsin \sqrt{\tau} & \tau \geq 1 \\ \frac{\sqrt{1 - \tau^{-1}}}{2} \left[\log \frac{1 + \sqrt{1 - \tau^{-1}}}{1 - \sqrt{1 - \tau^{-1}}} - i\pi \right] & \tau < 1 \end{cases} \quad (25)$$

$\mathcal{F}_0^{h_1}(\tau_i, \lambda_i)$, $i = H_1^\pm, H_2^\pm, H^{\pm\pm}$ factors reflecting the charged contributions for $\Gamma_{\gamma Z}$ can be read in terms of the function $I_1(\tau, \lambda)$ previously defined as follows :

$$\mathcal{F}_0^{h_1}(\tau_{H_i^\pm}, \lambda_{H_i^\pm}) = 2I_1(\tau_{H_i^\pm}, \lambda_{H_i^\pm}) \quad i = 1, 2 \quad , \quad \mathcal{F}_0^{h_1}(\tau_{H^{\pm\pm}}, \lambda_{H^{\pm\pm}}) = 4I_1(\tau_{H^{\pm\pm}}, \lambda_{H^{\pm\pm}}) \quad (26)$$

with now $\tau_i = 4M_i^2/M_H^2$, $\lambda_i = 4M_i^2/M_Z^2$. Where the $\lambda_{ZH^\pm H_1^\mp}$, $\lambda_{ZH^\pm H_2^\mp}$, $\lambda_{ZH^{\pm\pm} H^\mp H^\mp}$ trilinear couplings can be expressed as :

$$\lambda_{ZH_1^\pm H_1^\mp} = [(c_w^2 - s_w^2)(C_{21}^2 + C_{22}^2) - 2s_w^2 C_{23}^2]/(s_w c_w) \quad (27)$$

$$\lambda_{ZH_2^\pm H_2^\mp} = [(c_w^2 - s_w^2)(C_{31}^2 + C_{32}^2) - 2s_w^2 C_{33}^2]/(s_w c_w) \quad (28)$$

$$\lambda_{ZH^{\pm\pm} H^\mp H^\mp} = 4(c_w^2 - s_w^2)/(s_w c_w) \quad (29)$$

where s_w and c_w are the sine and cosine of the Weinberg angle (θ_w), respectively.

B The Higgs sector

The bilinear part of the Higgs potential in Eq.2 is given by:

$$\begin{aligned} V_{H_1, H_2, \Delta}^{(2)} &= \frac{1}{2} (\rho_1, \rho_2, \delta^0) \mathcal{M}_{\mathcal{CP}_{even}}^2 \begin{pmatrix} \rho_1 \\ \rho_2 \\ \rho_0 \end{pmatrix} + \frac{1}{2} (\eta_1, \eta_2, \eta_0) \mathcal{M}_{\mathcal{CP}_{odd}}^2 \begin{pmatrix} \eta_1 \\ \eta_2 \\ \eta_0 \end{pmatrix} \\ &+ (\phi_1^-, \phi_2^-, \delta^-) \mathcal{M}_{\pm}^2 \begin{pmatrix} \phi_1^+ \\ \phi_2^+ \\ \delta^+ \end{pmatrix} + \delta^{++} \mathcal{M}_{\pm\pm}^2 \delta^{--} \dots, \end{aligned} \quad (30)$$

In the subsequent appendices, the elements of these mass matrices are explicitly presented.

B.1 The Scalar sector

In the CP-even scalar sector, the mixing of the states (ρ_1, ρ_2, ρ_0) leads to a total of three CP-even physical Higgs bosons (h_1, h_2, h_3) . The neutral scalar mass matrix reads :

$$\mathcal{M}_{\mathcal{CP}_{even}}^2 = \begin{pmatrix} m_{\rho_1 \rho_1}^2 & m_{\rho_2 \rho_1}^2 & m_{\rho_0 \rho_1}^2 \\ m_{\rho_1 \rho_2}^2 & m_{\rho_2 \rho_2}^2 & m_{\rho_0 \rho_2}^2 \\ m_{\rho_1 \rho_0}^2 & m_{\rho_2 \rho_0}^2 & m_{\rho_0 \rho_0}^2 \end{pmatrix} \quad (31)$$

Its diagonal terms are,

$$m_{\rho_1 \rho_1}^2 = \lambda_1 v_1^2 + \frac{v_2 (\sqrt{2} m_3^2 + \mu_3 v_t)}{\sqrt{2} v_1}$$

$$\begin{aligned}
m_{\rho_2\rho_2}^2 &= \lambda_2 v_2^2 + \frac{v_1 (\sqrt{2}m_3^2 + \mu_3 v_t)}{\sqrt{2}v_2} \\
m_{\rho_0\rho_0}^2 &= \frac{4(\bar{\lambda}_8 + \bar{\lambda}_9) v_t^3 + \sqrt{2}(\mu_1 v_1^2 + \mu_3 v_2 v_1 + \mu_2 v_2^2)}{2v_t}
\end{aligned} \tag{32}$$

and the off-diagonal terms are defined by,

$$\begin{aligned}
m_{\rho_2\rho_1}^2 &= m_{\rho_1\rho_2}^2 = \frac{1}{\sqrt{2}} \left(\sqrt{2}v_1 v_2 \lambda_{345} - \sqrt{2}m_3^2 - \mu_3 v_t \right) \\
m_{\rho_0\rho_1}^2 &= m_{\rho_1\rho_0}^2 = \frac{1}{\sqrt{2}} \left(\sqrt{2}v_1 v_t (\lambda_6 + \lambda_8) - (2\mu_1 v_1 + \mu_3 v_2) \right) \\
m_{\rho_0\rho_2}^2 &= m_{\rho_2\rho_0}^2 = \frac{1}{\sqrt{2}} \left(\sqrt{2}v_2 v_t (\lambda_7 + \lambda_9) - (2\mu_2 v_2 + \mu_3 v_1) \right)
\end{aligned} \tag{33}$$

The mass matrix can be diagonalized using an orthogonal matrix \mathcal{E} parameterized as follows:

$$\mathcal{E} = \begin{pmatrix} c_{\alpha_1} c_{\alpha_2} & s_{\alpha_1} c_{\alpha_2} & s_{\alpha_2} \\ -(c_{\alpha_1} s_{\alpha_2} s_{\alpha_3} + s_{\alpha_1} c_{\alpha_3}) & c_{\alpha_1} c_{\alpha_3} - s_{\alpha_1} s_{\alpha_2} s_{\alpha_3} & c_{\alpha_2} s_{\alpha_3} \\ -c_{\alpha_1} s_{\alpha_2} c_{\alpha_3} + s_{\alpha_1} s_{\alpha_3} & -(c_{\alpha_1} s_{\alpha_3} + s_{\alpha_1} s_{\alpha_2} c_{\alpha_3}) & c_{\alpha_2} c_{\alpha_3} \end{pmatrix} \tag{34}$$

where the mixing angles α_1 , α_2 and α_3 are in the range

$$-\frac{\pi}{2} \leq \alpha_{1,2,3} \leq \frac{\pi}{2}. \tag{35}$$

the rotation between the two basis (ρ_1, ρ_2, ρ_0) and (h_1, h_2, h_3) diagonalizes the mass matrix $\mathcal{M}_{\mathcal{CP}_{even}}^2$ as,

$$\mathcal{E} \mathcal{M}_{\mathcal{CP}_{even}}^2 \mathcal{E}^T = \text{diag}(m_{h_1}^2, m_{h_2}^2, m_{h_3}^2) \tag{36}$$

and leads to three mass eigenstates, ordered by ascending mass as:

$$m_{h_1}^2 < m_{h_2}^2 < m_{h_3}^2. \tag{37}$$

B.2 The Charged Sector

Mass of the doubly charged bosons

The doubly charged mass $m_{H^{\pm\pm}}^2$, corresponding to the doubly charged eigenstate $\delta^{\pm\pm}$, can simply be determined by collecting all the coefficients of $\delta^{++}\delta^{--}$ in the scalar potential. When that is done the mass reads,

$$m_{H^{\pm\pm}}^2 = \frac{\sqrt{2}\mu_1 v_1^2 + \sqrt{2}\mu_3 v_1 v_2 + \sqrt{2}\mu_2 v_2^2 - \lambda_8 v_1^2 v_t - \lambda_9 v_2^2 v_t - 2\bar{\lambda}_9 v_t^3}{2v_t} \tag{38}$$

Mass of the simply charged bosons

In the Charged scalar sector, the mixing of the states $(\phi_1^\pm, \phi_2^\pm, \delta^\pm)$ leads to a total of three charged states, $(G^\pm, H_1^\pm, H_2^\pm)$. The rotation between the physical and non-physical states can be repre-

sented as :

$$\begin{pmatrix} G^\pm \\ H_1^\pm \\ H_2^\pm \end{pmatrix} = \mathcal{C} \begin{pmatrix} \phi_1^\pm \\ \phi_2^\pm \\ \delta^\pm \end{pmatrix} \quad (39)$$

The mass-squared matrix for the simply charged field in the $(\phi_1^-, \phi_2^-, \delta^-)$ basis reads as:

$$\mathcal{M}_\pm^2 = \begin{pmatrix} \mathcal{M}_{11}^\pm & \frac{1}{2}(\lambda_{45}^+ v_1 v_2 - 2m_3^2) & \frac{1}{4}(v_1 A - 2\mu_3 v_2) \\ \frac{1}{2}(\lambda_{45}^+ v_1 v_2 - 2m_3^2) & \mathcal{M}_{22}^\pm & \frac{1}{4}(v_2 B - 2\mu_3 v_1) \\ \frac{1}{4}(v_1 A - 2\mu_3 v_2) & \frac{1}{4}(v_2 B - 2\mu_3 v_1) & \mathcal{M}_{33}^\pm \end{pmatrix} \quad (40)$$

where $A = \sqrt{2}\lambda_8 v_t - 4\mu_1$, $B = \sqrt{2}\lambda_9 v_t - 4\mu_2$ while the diagonal terms read as,

$$\begin{aligned} \mathcal{M}_{11}^\pm &= \frac{2m_3^2 v_2 + v_1 v_t (2\sqrt{2}\mu_1 - \lambda_8 v_t) + \sqrt{2}\mu_3 v_2 v_t - \lambda_{45}^+ v_1 v_2^2}{2v_1} \\ \mathcal{M}_{22}^\pm &= \frac{2m_3^2 v_1 + v_2 v_t (2\sqrt{2}\mu_2 - \lambda_9 v_t) + \sqrt{2}\mu_3 v_1 v_t - \lambda_{45}^+ v_1^2 v_2}{2v_2} \\ \mathcal{M}_{33}^\pm &= \frac{v_1^2 (2\sqrt{2}\mu_1 - \lambda_8 v_t) + v_2^2 (2\sqrt{2}\mu_2 - \lambda_9 v_t) + 2\sqrt{2}\mu_3 v_2 v_1 - 2\bar{\lambda}_9 v_t^3}{4v_t} \end{aligned} \quad (41)$$

Among the three eigenvalues of the matrix \mathcal{M}_\pm^2 , one is zero and corresponds to the charged Goldstone boson G^\pm , The remaining two eigenvalues correspond to the singly charged Higgs bosons, denoted as $m_{H_1^\pm}^2$ and $m_{H_2^\pm}^2$ and are given by,

$$m_{H_{1,2}^\pm}^2 = \frac{1}{4v_0^2 v_t} \left[-v_0 \left(v_0 (2\mathcal{M}_{12}^\pm \text{cs}_\beta \text{se}_\beta v_t + \kappa) + 2\sqrt{2}v_t^2 (\mathcal{M}_{23}^\pm \text{cs}_\beta + \mathcal{M}_{13}^\pm \text{se}_\beta) \right) \mp \text{cs}_\beta \text{se}_\beta \sqrt{\mathcal{Y}} \right] \quad (42)$$

where $c_x, s_x, \text{cs}_x, \text{se}_x$ stand for the $\cos(x), \sin(x), \csc(x), \sec(x)$ respectively, while $v_0 = \sqrt{v_1^2 + v_2^2}$, $v = \sqrt{v_1^2 + v_2^2 + 2v_t^2}$, $\kappa = \sqrt{2}v_0 (\mathcal{M}_{13}^\pm c_\beta + \mathcal{M}_{23}^\pm s_\beta)$ and

$$\begin{aligned} \mathcal{Y} &= v_0^2 \left((v_0 (\kappa c_\beta s_\beta + 2\mathcal{M}_{12}^\pm v_t) + 2\sqrt{2}v_t^2 (\mathcal{M}_{23}^\pm c_\beta + \mathcal{M}_{13}^\pm s_\beta))^2 \right. \\ &\quad \left. - 4v^2 s_{2\beta} v_t (\kappa \mathcal{M}_{12}^\pm + 2\mathcal{M}_{13}^\pm \mathcal{M}_{23}^\pm v_t) \right) \end{aligned} \quad (43)$$

The above symmetric squared matrix \mathcal{M}_\pm^2 can be diagonalized via \mathcal{C} as follows,

$$\mathcal{C} \mathcal{M}_\pm^2 \mathcal{C}^T = \text{diag}(m_{G^\pm}^2, m_{H_1^\pm}^2, m_{H_2^\pm}^2) \quad (44)$$

where the \mathcal{C} rotation matrix is described by three mixing angles $\theta_1^\pm, \theta_2^\pm$ and θ_3^\pm , and the corresponding expressions for the \mathcal{C} elements as a function of the input parameters of our model are given by,

$$\mathcal{C} = \begin{pmatrix} \mathcal{C}_{11} & \mathcal{C}_{12} & \mathcal{C}_{13} \\ \mathcal{C}_{21} & \mathcal{C}_{22} & \mathcal{C}_{23} \\ \mathcal{C}_{31} & \mathcal{C}_{32} & \mathcal{C}_{33} \end{pmatrix} = \begin{pmatrix} c_{\theta_1^\pm} c_{\theta_2^\pm} & s_{\theta_1^\pm} c_{\theta_2^\pm} & s_{\theta_2^\pm} \\ -(c_{\theta_1^\pm} s_{\theta_2^\pm} s_{\theta_3^\pm} + s_{\theta_1^\pm} c_{\theta_3^\pm}) & c_{\theta_1^\pm} c_{\theta_3^\pm} - s_{\theta_1^\pm} s_{\theta_2^\pm} s_{\theta_3^\pm} & c_{\theta_2^\pm} s_{\theta_3^\pm} \\ -c_{\theta_1^\pm} s_{\theta_2^\pm} c_{\theta_3^\pm} + s_{\theta_1^\pm} s_{\theta_3^\pm} & -(c_{\theta_1^\pm} s_{\theta_3^\pm} + s_{\theta_1^\pm} s_{\theta_2^\pm} c_{\theta_3^\pm}) & c_{\theta_2^\pm} c_{\theta_3^\pm} \end{pmatrix} \quad (45)$$

$$\mathcal{C}_{11} = \frac{v_1}{v}, \quad \mathcal{C}_{12} = \frac{v_2}{v}, \quad \mathcal{C}_{13} = \sqrt{2} \frac{v_t}{v} \quad (46)$$

$$\mathcal{C}_{21} = \frac{x_1}{\sqrt{\mathcal{N}}}, \quad \mathcal{C}_{22} = \frac{x_2}{\sqrt{\mathcal{N}}}, \quad \mathcal{C}_{23} = \frac{1}{\sqrt{\mathcal{N}}} \quad (47)$$

$$\mathcal{C}_{31} = \mathcal{C}_{21}[m_{H_1^\pm}^2 \rightarrow m_{H_2^\pm}^2], \quad \mathcal{C}_{32} = \mathcal{C}_{22}[m_{H_1^\pm}^2 \rightarrow m_{H_2^\pm}^2], \quad \mathcal{C}_{33} = \mathcal{C}_{23}[m_{H_1^\pm}^2 \rightarrow m_{H_2^\pm}^2] \quad (48)$$

where $v_0 = \sqrt{v_1^2 + v_2^2}$ and

$$x_1 = \frac{v_0 c_\beta \left(v_0 \left(\mathcal{M}_{12}^\pm (\mathcal{M}_{13}^\pm c_\beta + \mathcal{M}_{23}^\pm s_\beta) + \mathcal{M}_{13}^\pm m_{H_1^\pm}^2 s_\beta \right) + \sqrt{2} \mathcal{M}_{13}^\pm \mathcal{M}_{23}^\pm v_t \right)}{\sqrt{2} v_0 v_t \left(m_{H_1^\pm}^2 (\mathcal{M}_{23}^\pm c_\beta + \mathcal{M}_{13}^\pm s_\beta) + \mathcal{M}_{12}^\pm (\mathcal{M}_{13}^\pm c_\beta + \mathcal{M}_{23}^\pm s_\beta) \right) + v_0^2 m_{H_1^\pm}^2 \left(c_\beta m_{H_1^\pm}^2 s_\beta + \mathcal{M}_{12}^\pm \right) + 2 \mathcal{M}_{13}^\pm \mathcal{M}_{23}^\pm v_t^2} \quad (49)$$

$$x_2 = \frac{v_0 s_\beta \left(\mathcal{M}_{23}^\pm \left(v_0 c_\beta m_{H_1^\pm}^2 + \sqrt{2} \mathcal{M}_{13}^\pm v_t \right) + \mathcal{M}_{12}^\pm v_0 (\mathcal{M}_{13}^\pm c_\beta + \mathcal{M}_{23}^\pm s_\beta) \right)}{\sqrt{2} v_0 v_t \left(m_{H_1^\pm}^2 (\mathcal{M}_{23}^\pm c_\beta + \mathcal{M}_{13}^\pm s_\beta) + \mathcal{M}_{12}^\pm (\mathcal{M}_{13}^\pm c_\beta + \mathcal{M}_{23}^\pm s_\beta) \right) + v_0^2 m_{H_1^\pm}^2 \left(c_\beta m_{H_1^\pm}^2 s_\beta + \mathcal{M}_{12}^\pm \right) + 2 \mathcal{M}_{13}^\pm \mathcal{M}_{23}^\pm v_t^2} \quad (50)$$

$$\mathcal{N} = \sqrt{1 + x_1^2 + x_2^2} \quad (51)$$

For the input parameters implemented in *2HDMcT*, we used the following hybrid parametrization,

$$\mathcal{P}_I = \{ \alpha_1, \alpha_2, \alpha_3, m_{h_1}, m_{h_2}, m_{h_3}, m_{H^{\pm\pm}}, \lambda_1, \lambda_3, \lambda_4, \lambda_6, \lambda_8, \bar{\lambda}_8, \bar{\lambda}_9, \mu_1, v_t, \tan \beta \} \quad (52)$$

with $\tan \beta = v_2/v_1$. One can easily express the set of Lagrangian parameters in Eq.2 in terms of those given by 52.

$$\begin{aligned} \lambda_2 &= \frac{-\mathcal{B}c_\beta^2 + \lambda_1 v_0^2 c_\beta^4 + (\mathcal{E}_{12}^2 m_{h_1}^2 + \mathcal{E}_{22}^2 m_{h_2}^2 + \mathcal{E}_{32}^2 m_{h_3}^2) s_\beta^2}{v_0^2 s_\beta^4} \\ \lambda_5 &= \frac{(\mathcal{B} - \lambda_{34}^+ v_0^2 s_\beta^2) c_\beta - \lambda_1 v_0^2 c_\beta^3 + (\mathcal{E}_{11} \mathcal{E}_{12} m_{h_1}^2 + \mathcal{E}_{21} \mathcal{E}_{22} m_{h_2}^2 + \mathcal{E}_{31} \mathcal{E}_{32} m_{h_3}^2) s_\beta}{v_0^2 c_\beta s_\beta^2} \\ \lambda_9 &= \frac{-\lambda_8 v_0^2 c_\beta^2 + 2\mathcal{F} - 2m_{H^{\pm\pm}}^2 - 2(2\bar{\lambda}_8 + 3\bar{\lambda}_9) v_t^2}{v_0^2 s_\beta^2} \\ \lambda_7 &= \frac{v_0 (\mathcal{A}c_\beta + \mathcal{M}s_\beta) + v_t \left(-\lambda_6 v_0^2 c_\beta^2 - 2\mathcal{F} + 2m_{H^{\pm\pm}}^2 + 2(2\bar{\lambda}_8 + 3\bar{\lambda}_9) v_t^2 \right)}{v_0^2 s_\beta^2 v_t} \\ \mu_2 &= \frac{c_\beta (2\mathcal{A} + v_0 c_\beta (\sqrt{2}\mu_1 - 2\lambda_{68}^+ v_t))}{\sqrt{2} v_0 s_\beta^2} \\ \mu_3 &= \frac{\sqrt{2} \left(-\mathcal{A}v_0 c_\beta + v_0^2 c_\beta^2 (\lambda_{68}^+ v_t - \sqrt{2}\mu_1) + v_t (\mathcal{E}_{13}^2 m_{h_1}^2 + \mathcal{E}_{23}^2 m_{h_2}^2 + \mathcal{E}_{33}^2 m_{h_3}^2 - 2\bar{\lambda}_{89}^+ v_t^2) \right)}{v_0^2 c_\beta s_\beta} \\ m_3^2 &= \frac{\mathcal{A}v_t + v_0 c_\beta (\mathcal{B} - v_t (\lambda_{68}^+ v_t - \sqrt{2}\mu_1)) - \lambda_1 v_0^3 c_\beta^3}{v_0 s_\beta} \quad (53) \end{aligned}$$

where $v_0 = \sqrt{v_1^2 + v_2^2}$ and

$$\begin{aligned}
\mathcal{A} &= \mathcal{E}_{11}\mathcal{E}_{13}m_{h_1}^2 + \mathcal{E}_{21}\mathcal{E}_{23}m_{h_2}^2 + \mathcal{E}_{31}\mathcal{E}_{33}m_{h_3}^2 \\
\mathcal{B} &= \mathcal{E}_{11}^2m_{h_1}^2 + \mathcal{E}_{21}^2m_{h_2}^2 + \mathcal{E}_{31}^2m_{h_3}^2 \\
\mathcal{F} &= \mathcal{E}_{13}^2m_{h_1}^2 + \mathcal{E}_{23}^2m_{h_2}^2 + \mathcal{E}_{33}^2m_{h_3}^2 \\
\mathcal{M} &= \mathcal{E}_{12}\mathcal{E}_{13}m_{h_1}^2 + \mathcal{E}_{22}\mathcal{E}_{23}m_{h_2}^2 + \mathcal{E}_{32}\mathcal{E}_{33}m_{h_3}^2
\end{aligned} \tag{54}$$

References

- [1] **ATLAS** Collaboration, G. Aad et al., *Observation of a new particle in the search for the Standard Model Higgs boson with the ATLAS detector at the LHC*, *Phys. Lett. B* **716** (2012) 1–29, [[arXiv:1207.7214](#)].
- [2] **CMS** Collaboration, S. Chatrchyan et al., *Observation of a New Boson at a Mass of 125 GeV with the CMS Experiment at the LHC*, *Phys. Lett. B* **716** (2012) 30–61, [[arXiv:1207.7235](#)].
- [3] **CMS** Collaboration, A. Tumasyan et al., *A portrait of the Higgs boson by the CMS experiment ten years after the discovery.*, *Nature* **607** (2022), no. 7917 60–68, [[arXiv:2207.00043](#)].
- [4] **ATLAS** Collaboration, G. Aad et al., *A detailed map of Higgs boson interactions by the ATLAS experiment ten years after the discovery*, *Nature* **607** (2022), no. 7917 52–59, [[arXiv:2207.00092](#)]. [Erratum: *Nature* 612, E24 (2022)].
- [5] W. Elmetenawee, *Summary of CMS Higgs Physics*, [arXiv:2401.07650](#).
- [6] F. Zwicky, *Die Rotverschiebung von extragalaktischen Nebeln*, *Helv. Phys. Acta* **6** (1933) 110–127.
- [7] V. C. Rubin and W. K. Ford, Jr., *Rotation of the Andromeda Nebula from a Spectroscopic Survey of Emission Regions*, *Astrophys. J.* **159** (1970) 379–403.
- [8] M. J. G. Veltman, *The Infrared - Ultraviolet Connection*, *Acta Phys. Polon. B* **12** (1981) 437.
- [9] T. Kajita, *Nobel lecture: Discovery of atmospheric neutrino oscillations*, *Rev. Mod. Phys.* **88** (Jul, 2016) 030501.
- [10] A. B. McDonald, *Nobel lecture: The sudbury neutrino observatory: Observation of flavor change for solar neutrinos*, *Rev. Mod. Phys.* **88** (Jul, 2016) 030502.
- [11] N. G. Deshpande and E. Ma, *Pattern of Symmetry Breaking with Two Higgs Doublets*, *Phys. Rev. D* **18** (1978) 2574.
- [12] S. L. Glashow and S. Weinberg, *Natural conservation laws for neutral currents*, *Phys. Rev. D* **15** (Apr, 1977) 1958–1965.
- [13] G. C. Branco, P. M. Ferreira, L. Lavoura, M. N. Rebelo, M. Sher, and J. P. Silva, *Theory and phenomenology of two-Higgs-doublet models*, *Phys. Rept.* **516** (2012) 1–102, [[arXiv:1106.0034](#)].
- [14] S. Dawson, C. Englert, and T. Plehn, *Higgs Physics: It ain't over till it's over*, *Phys. Rept.* **816** (2019) 1–85, [[arXiv:1808.01324](#)].
- [15] I. P. Ivanov, *Building and testing models with extended Higgs sectors*, *Prog. Part. Nucl. Phys.* **95** (2017) 160–208, [[arXiv:1702.03776](#)].
- [16] S. Weinberg, *Baryon- and lepton-nonconserving processes*, *Phys. Rev. Lett.* **43** (Nov, 1979) 1566–1570.
- [17] B. Ait Ouazghour, A. Arhrib, R. Benbrik, M. Chabab, and L. Rahili, *Theory and phenomenology of a two-Higgs-doublet type-II seesaw model at the LHC run 2*, *Phys. Rev. D* **100** (2019), no. 3 035031, [[arXiv:1812.07719](#)].
- [18] B. Ait Ouazghour and M. Chabab, *The two Higgs doublet type-II seesaw model: Naturalness and $B^- \rightarrow Xs\gamma$ versus heavy Higgs masses*, *Phys. Lett. B* **846** (2023) 138241, [[arXiv:2305.08030](#)].

- [19] **ATLAS** Collaboration, M. Aaboud et al., *Search for additional heavy neutral Higgs and gauge bosons in the ditau final state produced in 36 fb^{-1} of pp collisions at $\sqrt{s} = 13 \text{ TeV}$ with the ATLAS detector*, *JHEP* **01** (2018) 055, [[arXiv:1709.07242](#)].
- [20] **ATLAS** Collaboration, M. Aaboud et al., *Search for new phenomena in high-mass diphoton final states using 37 fb^{-1} of proton–proton collisions collected at $\sqrt{s} = 13 \text{ TeV}$ with the ATLAS detector*, *Phys. Lett. B* **775** (2017) 105–125, [[arXiv:1707.04147](#)].
- [21] **CMS** Collaboration, A. M. Sirunyan et al., *Search for a new scalar resonance decaying to a pair of Z bosons in proton-proton collisions at $\sqrt{s} = 13 \text{ TeV}$* , *JHEP* **06** (2018) 127, [[arXiv:1804.01939](#)]. [Erratum: *JHEP* 03, 128 (2019)].
- [22] **ATLAS** Collaboration, M. Aaboud et al., *Search for a heavy Higgs boson decaying into a Z boson and another heavy Higgs boson in the $\ell\ell b\bar{b}$ final state in pp collisions at $\sqrt{s} = 13 \text{ TeV}$ with the ATLAS detector*, *Phys. Lett. B* **783** (2018) 392–414, [[arXiv:1804.01126](#)].
- [23] **CMS** Collaboration, A. M. Sirunyan et al., *Search for heavy Higgs bosons decaying to a top quark pair in proton-proton collisions at $\sqrt{s} = 13 \text{ TeV}$* , *JHEP* **04** (2020) 171, [[arXiv:1908.01115](#)]. [Erratum: *JHEP* 03, 187 (2022)].
- [24] **CMS** Collaboration, A. M. Sirunyan et al., *Search for MSSM Higgs bosons decaying to $\mu + \mu -$ in proton-proton collisions at $s=13\text{TeV}$* , *Phys. Lett. B* **798** (2019) 134992, [[arXiv:1907.03152](#)].
- [25] **CMS** Collaboration, *Search for a charged Higgs boson decaying into a heavy neutral Higgs boson and a W boson in proton-proton collisions at $\sqrt{s} = 13 \text{ TeV}$* , *arXiv e-prints* (July, 2022) [arXiv:2207.01046](#), [[arXiv:2207.01046](#)].
- [26] R. S. Gupta, H. Rzehak, and J. D. Wells, *How well do we need to measure the Higgs boson mass and self-coupling?*, *Phys. Rev. D* **88** (2013) 055024, [[arXiv:1305.6397](#)].
- [27] J. Baglio and C. Weiland, *The triple Higgs coupling: A new probe of low-scale seesaw models*, *JHEP* **04** (2017) 038, [[arXiv:1612.06403](#)].
- [28] **ILC physics, detector study** Collaboration, J. Tian and K. Fujii, *Measurement of Higgs boson couplings at the International Linear Collider*, *Nucl. Part. Phys. Proc.* **273-275** (2016) 826–833.
- [29] C. F. Dürig, *Measuring the Higgs Self-coupling at the International Linear Collider*. PhD thesis, Hamburg U., Hamburg, 2016.
- [30] T. Liu, K.-F. Lyu, J. Ren, and H. X. Zhu, *Probing the quartic Higgs boson self-interaction*, *Phys. Rev. D* **98** (2018), no. 9 093004, [[arXiv:1803.04359](#)].
- [31] A. Arbey et al., *Physics at the $e+ e-$ Linear Collider*, *Eur. Phys. J. C* **75** (2015), no. 8 371, [[arXiv:1504.01726](#)].
- [32] **ILC International Development Team** Collaboration, A. Aryshev et al., *The International Linear Collider: Report to Snowmass 2021*, [arXiv:2203.07622](#).
- [33] P. Bambade et al., *The International Linear Collider: A Global Project*, [arXiv:1903.01629](#).
- [34] **CLIC Physics Working Group** Collaboration, E. Accomando et al., *Physics at the CLIC multi-TeV linear collider*, in *11th International Conference on Hadron Spectroscopy*, CERN Yellow Reports: Monographs, 6, 2004. [hep-ph/0412251](#).
- [35] **CEPC Study Group** Collaboration, *CEPC Conceptual Design Report: Volume 1 - Accelerator*, [arXiv:1809.00285](#).
- [36] **CEPC Study Group** Collaboration, M. Dong et al., *CEPC Conceptual Design Report: Volume 2 - Physics & Detector*, [arXiv:1811.10545](#).
- [37] **CEPC Study Group** Collaboration, W. Abdallah et al., *CEPC Technical Design Report - Accelerator*, [arXiv:2312.14363](#).
- [38] **TLEP Design Study Working Group** Collaboration, M. Bicer et al., *First Look at the Physics Case of TLEP*, *JHEP* **01** (2014) 164, [[arXiv:1308.6176](#)].
- [39] **FCC** Collaboration, A. Abada et al., *FCC Physics Opportunities: Future Circular Collider Conceptual Design Report Volume 1*, *Eur. Phys. J. C* **79** (2019), no. 6 474.
- [40] **LCC Physics Working Group** Collaboration, K. Fujii et al., *Tests of the Standard Model at the International Linear Collider*, [arXiv:1908.11299](#).

- [41] A. Abbasabadi, D. Bowser-Chao, D. A. Dicus, and W. W. Repko, *Higgs-boson–photon associated production at $e\bar{e}$ colliders*, *Phys. Rev. D* **52** (Oct, 1995) 3919–3928.
- [42] A. Djouadi, V. Driesen, W. Hollik, and J. Rosiek, *Associated production of Higgs bosons and a photon in high-energy e^+e^- collisions*, *Nuclear Physics B* **491** (Feb., 1997) 68–102, [[hep-ph/9609420](#)].
- [43] A. Barroso, J. Pulido, and J. C. Romao, *HIGGS PRODUCTION AT e^+e^- COLLIDERS*, *Nucl. Phys. B* **267** (1986) 509–530.
- [44] A. Arhrib, R. Benbrik, and T.-C. Yuan, *Associated Production of Higgs at Linear Collider in the Inert Higgs Doublet Model*, *Eur. Phys. J. C* **74** (2014) 2892, [[arXiv:1401.6698](#)].
- [45] L. Rahili, A. Arhrib, and R. Benbrik, *Associated production of SM Higgs with a photon in type-II seesaw models at the ILC*, *Eur. Phys. J. C* **79** (2019), no. 11 940, [[arXiv:1909.07793](#)].
- [46] S. Heinemeyer and C. Schappacher, *Neutral Higgs boson production at e^+e^- colliders in the complex MSSM: a full one-loop analysis*, *European Physical Journal C* **76** (Apr., 2016) 220, [[arXiv:1511.06002](#)].
- [47] M. Demirci, *Associated production of Higgs boson with a photon at electron-positron colliders*, *Phys. Rev. D* **100** (2019), no. 7 075006, [[arXiv:1905.09363](#)].
- [48] **ILD concept group** Collaboration, Y. Aoki, K. Fujii, and J. Tian, *Study of $e^+e^- \rightarrow \gamma h$ at the ILC*, [[arXiv:2203.07202](#)].
- [49] C.-H. Chen and T. Nomura, *Inert Dark Matter in Type-II Seesaw*, *JHEP* **09** (2014) 120, [[arXiv:1404.2996](#)].
- [50] P. Fileviez Perez, T. Han, G.-y. Huang, T. Li, and K. Wang, *Neutrino Masses and the CERN LHC: Testing Type II Seesaw*, *Phys. Rev. D* **78** (2008) 015018, [[arXiv:0805.3536](#)].
- [51] Y. Cai, T. Han, T. Li, and R. Ruiz, *Lepton Number Violation: Seesaw Models and Their Collider Tests*, *Front. in Phys.* **6** (2018) 40, [[arXiv:1711.02180](#)].
- [52] S. F. King, *Models of Neutrino Mass, Mixing and CP Violation*, *J. Phys. G* **42** (2015) 123001, [[arXiv:1510.02091](#)].
- [53] S. Ashanujjaman and K. Ghosh, *Revisiting type-II see-saw: present limits and future prospects at LHC*, *JHEP* **03** (2022) 195, [[arXiv:2108.10952](#)].
- [54] M. J. Ramsey-Musolf, *The electroweak phase transition: a collider target*, *JHEP* **09** (2020) 179, [[arXiv:1912.07189](#)].
- [55] M. E. Peskin and T. Takeuchi, *Estimation of oblique electroweak corrections*, *Phys. Rev.* **D46** (1992) 381–409.
- [56] W. Grimus, L. Lavoura, O. M. Ogreid, and P. Osland, *The Oblique parameters in multi-Higgs-doublet models*, *Nucl. Phys. B* **801** (2008) 81–96, [[arXiv:0802.4353](#)].
- [57] **Particle Data Group** Collaboration, R. L. Workman et al., *Review of Particle Physics*, *PTEP* **2022** (2022) 083C01.
- [58] H. Bahl, T. Biekötter, S. Heinemeyer, C. Li, S. Paasch, G. Weiglein, and J. Wittbrodt, *HiggsTools: BSM scalar phenomenology with new versions of HiggsBounds and HiggsSignals*, *Comput. Phys. Commun.* **291** (2023) 108803, [[arXiv:2210.09332](#)].
- [59] P. Bechtle, S. Heinemeyer, O. Stål, T. Stefaniak, and G. Weiglein, *HiggsSignals: Confronting arbitrary Higgs sectors with measurements at the Tevatron and the LHC*, *Eur. Phys. J. C* **74** (2014), no. 2 2711, [[arXiv:1305.1933](#)].
- [60] P. Bechtle, S. Heinemeyer, O. Stål, T. Stefaniak, and G. Weiglein, *Probing the Standard Model with Higgs signal rates from the Tevatron, the LHC and a future ILC*, *JHEP* **11** (2014) 039, [[arXiv:1403.1582](#)].
- [61] P. Bechtle, S. Heinemeyer, T. Klingl, T. Stefaniak, G. Weiglein, and J. Wittbrodt, *HiggsSignals-2: Probing new physics with precision Higgs measurements in the LHC 13 TeV era*, *Eur. Phys. J. C* **81** (2021), no. 2 145, [[arXiv:2012.09197](#)].
- [62] P. Bechtle, O. Brein, S. Heinemeyer, G. Weiglein, and K. E. Williams, *HiggsBounds: Confronting Arbitrary Higgs Sectors with Exclusion Bounds from LEP and the Tevatron*, *Comput. Phys. Commun.* **181** (2010) 138–167, [[arXiv:0811.4169](#)].

- [63] P. Bechtle, O. Brein, S. Heinemeyer, G. Weiglein, and K. E. Williams, *HiggsBounds 2.0.0: Confronting Neutral and Charged Higgs Sector Predictions with Exclusion Bounds from LEP and the Tevatron*, *Comput. Phys. Commun.* **182** (2011) 2605–2631, [[arXiv:1102.1898](#)].
- [64] P. Bechtle, O. Brein, S. Heinemeyer, O. Stål, T. Stefaniak, G. Weiglein, and K. E. Williams, *HiggsBounds – 4: Improved Tests of Extended Higgs Sectors against Exclusion Bounds from LEP, the Tevatron and the LHC*, *Eur. Phys. J. C* **74** (2014), no. 3 2693, [[arXiv:1311.0055](#)].
- [65] P. Bechtle, D. Dercks, S. Heinemeyer, T. Klingl, T. Stefaniak, G. Weiglein, and J. Wittbrodt, *HiggsBounds-5: Testing Higgs Sectors in the LHC 13 TeV Era*, *Eur. Phys. J. C* **80** (2020), no. 12 1211, [[arXiv:2006.06007](#)].
- [66] **HFLAV** Collaboration, Y. S. Amhis et al., *Averages of b -hadron, c -hadron, and τ -lepton properties as of 2021*, *Phys. Rev. D* **107** (2023) 052008, [[arXiv:2206.07501](#)].
- [67] T. Hahn, *Generating Feynman diagrams and amplitudes with FeynArts 3*, *Comput. Phys. Commun.* **140** (2001) 418–431, [[hep-ph/0012260](#)].
- [68] T. Hahn and M. Pérez-Victoria, *Automated one-loop calculations in four and d dimensions*, *Computer Physics Communications* **118** (1999), no. 2 153–165.
- [69] G. J. van Oldenborgh, *FF: A Package to evaluate one loop Feynman diagrams*, *Comput. Phys. Commun.* **66** (1991) 1–15.
- [70] T. Hahn, *Feynman Diagram Calculations with FeynArts, FormCalc, and LoopTools*, *PoS ACAT2010* (2010) 078, [[arXiv:1006.2231](#)].
- [71] **ATLAS** Collaboration, G. Aad et al., *Measurement of the properties of Higgs boson production at $\sqrt{s} = 13$ TeV in the $H \rightarrow \gamma\gamma$ channel using 139 fb^{-1} of pp collision data with the ATLAS experiment*, *JHEP* **07** (2023) 088, [[arXiv:2207.00348](#)].
- [72] **ATLAS** Collaboration, G. Aad et al., *A search for the $Z\gamma$ decay mode of the Higgs boson in pp collisions at $\sqrt{s} = 13$ TeV with the ATLAS detector*, *Phys. Lett. B* **809** (2020) 135754, [[arXiv:2005.05382](#)].
- [73] **CMS** Collaboration, A. Tumasyan et al., *Search for Higgs boson decays to a Z boson and a photon in proton-proton collisions at $\sqrt{s} = 13$ TeV*, *JHEP* **05** (2023) 233, [[arXiv:2204.12945](#)].
- [74] **CMS, ATLAS** Collaboration, G. Aad et al., *Evidence for the Higgs boson decay to a Z boson and a photon at the LHC*, [[arXiv:2309.03501](#)].
- [75] **ATLAS** Collaboration, G. Aad et al., *Search for the $Z\gamma$ decay mode of new high-mass resonances in pp collisions at $\sqrt{s} = 13$ TeV with the ATLAS detector*, [[arXiv:2309.04364](#)].